



Multilevel finite volume methods and boundary conditions for geophysical flows



Arthur Bousquet^a, Martine Marion^b, Madalina Petcu^{c,d}, Roger Temam^{a,*}

^aThe Institute for Scientific Computing and Applied Mathematics, Indiana University, Bloomington, IN 47405, USA

^bUniversité de Lyon, Ecole Centrale de Lyon, CNRS UMR 5208, DMI, 36 avenue Guy de Collongue, 69134 Ecully, France

^cLaboratoire de Mathématiques et Applications, UMR 6086, Université de Poitiers, France

^dThe Institute of Mathematics of the Romanian Academy, Bucharest, Romania

ARTICLE INFO

Article history:

Available online 11 January 2013

Keywords:

Finite volume
Central-upwind
Multi-level method
Transparent boundary conditions
Shallow water equations

ABSTRACT

This review article concerns multi-level methods for finite volume discretizations. They are presented in the context of the non-viscous shallow water equations in space dimension one and two, although the ideas are of more general validity. The second, partly related topic, addressed in this article is that of boundary conditions also presented in the context of the inviscid shallow water equations. Beside algorithmic presentation, the article contains the discussion of some numerical stability issues and the results of some numerical simulations. The multi-level method is applied numerically to the equations of shallow water using a central-upwind scheme for finite volumes and we prove the stability for the linear shallow water equations in different situations. The question of the boundary conditions is illustrated for the two-dimensional equations in the reference case of the so-called Rossby soliton.

© 2013 Elsevier Ltd. All rights reserved.

1. Introduction

In this review article we address two different related issues: the use of multi-level methods in the context of finite volume discretization and the problem of boundary conditions for nonlinear hyperbolic equations. Both issues are developed in the context of inviscid shallow water equations but the issues are clearly of much greater generality.

A class of multilevel methods, called Incremental Unknowns methods was introduced to improve calculation speed in the simulation of complex physical phenomena while maintaining an accurate solution of the problems. They were originally developed for the study of turbulent flows [23,25,26,52,53] but can be of interest as well in other types of problems encompassing many different scales.

Incremental unknowns were introduced in the context of spectral methods in [41,42]; see also [23,25,26,53]. They were extended to finite differences, finite elements and wavelets discretization in e.g. [52,16,14,21]. More recently the implementation of finite volume multilevel schemes for the solution of the Burgers equations with a diffusive term was made in [29]. It was developed also in [1] for the two-dimensional shallow water equations. The general principle is to split the unknowns in two (or more) terms: a “large-scale” component \mathbf{U} and one (or several) “small-scale” com-

ponent(s) \mathbf{Z} and to treat differently \mathbf{U} and \mathbf{Z} . The decomposition of the unknowns that we employ in this article is purely algebraic but it enables to preserve the numerical conservation of the scheme. The decomposition of the variables is here done globally but it can be done locally in certain parts of the domain only, based on physical motivations (or on information on the flow).

In Parts I and II of this article we are concerned with the solution of the two dimensional nonlinear shallow water equations by this multilevel method using finite volume discretization. This work is intended at exploring the implementation of such methods for this system. The shallow water system being hyperbolic, there is no diffusive term in the equations which could stabilize the scheme; however, as we shall see, the multilevel method that we present turns out to provide a good and efficient solution of the problem.

The shallow water equations describe the propagation of surface waves of long wavelength and of relatively large amplitude, which give rise to strongly nonlinear flows. Multilevel methods for the shallow water equations supplemented with a hyper-dissipative operator were studied in [26] in the context of spectral methods for the simulation of turbulence. Our study covers a general framework but we are particularly interested in the modeling of oceanic or atmospheric flows in the presence of mild turbulence. Therefore, unlike some other situations of physical interest (like e.g. the breakdown of a dam), the height is not meant to vanish, as in e.g. [4,5]. From this perspective we present simulations based on initial conditions taken from [26]. Our multilevel method allows

* Corresponding author. Tel.: +1 812 855 3807; fax: +1 812 855 7850.

E-mail address: temam@indiana.edu (R. Temam).

to resolve accurately the problems studied while reducing the CPU time and preserving the numerical conservation of the scheme.

For the spatial finite volume discretization, the hyperbolic nature of the system requires that we consider schemes that are well adapted to such problems. Recently, several finite volume schemes have been developed for the simulation of the shallow water equations [2–5,10,30,38,39,51,56] in order to study some particular properties (e.g. preservation of steady states, positivity of the height of the water). Here we apply a multilevel method built on central-upwind type schemes which were constructed to solve numerically nonlinear conservation laws, [36–38]. These Godunov-type schemes are based on exact evolution and averaging over Riemann fans and do not need the use of Riemann solvers and characteristic decomposition, which render them simple and efficient; moreover they can be reduced to a very simple semi-discrete form. More particularly we will work with the schemes presented in [37,38]: they are based on the one-sided local speeds of propagation and constitute less dissipative generalizations of the semi-discrete central-upwind schemes; they also allow to work on nonstaggered grids. However any finite volume scheme which can be written in a semi-discrete form can be used as well, provided that it is adapted to the hyperbolic nature of the system. Our method has been tested with central leap frog fluxes and the results were not satisfactory. For the time discretization we need to use a TVD method which preserves the spatial accuracy: in the simulations we employ a Runge Kutta method of order four. As stated above and as explained in more details below, our multilevel method is based on a different treatment of the large-scale and the small-scale components of the flow, the small-scale components being small in magnitude. For instances small-scale component of the variables can be calculated using a simple time scheme; in our experimentations we chose to freeze them. For the reader not familiar with these schemes, the puzzling terminology “central-upwind” is explained in Remark 7.

Section 2 (Part I) of this article is related to the article [1] and devoted to the practical implementation of a Finite Volume Incremental Unknowns (FVIU) with increments \mathbf{Z} of order two, that is $(\Delta x)^2$. Section 3 Part II which is related to the article [11] addresses some numerical analysis issues and is intended to studying the stability of some FVIU schemes. We are not able to prove the stability of the scheme of order two considered in in Part I. Instead we introduce two others FVIU schemes with increments \mathbf{Z} of order Δx . The stability of one scheme is studied by the spectral von Neumann method, the stability of the other scheme is studied by energy method. Many challenging issues remain open.

The multilevel schemes that we study have some similarities with algorithms commonly used in oceanography, a review of which appears in [22]. Similarities and differences are discussed in [1]. In particular several fundamental issues mentioned in [22] appear in our algorithms. One of them is the passage of information (values of the unknowns) from the coarse grid to the fine grid and back; this issue occurs in our algorithms; we have addressed it in Part I in a certain way consistent with earlier studies in finite volumes, but other procedures can be contemplated which we will investigate in the future if needed. In this work, the downward and upward passage of information appear in (4) and Remark 4. Another major issue mentioned in [22] is the boundary conditions at the boundary of the entire domain and at the boundary of each coarse cell when considering the refined cells that it contains. We do not study this problem per se but however address in Section 4 (Part III) a number of issues regarding the boundary conditions for the inviscid shallow water equations in relation with the article [13] and other more theoretical (mathematical) articles [47,48,32,33]. Indeed the question of boundary conditions for the inviscid shallow water equations is an essentially open problem, of current study; see new developments in the mathematical

articles we just quoted. For example the theoretical (mathematical) studies in [8,46] tend to show that the Dirichlet boundary conditions used in the standard test problem of the Rossby soliton that we consider in Part III are not suitable. This is numerically confirmed by the undesirable reflexions appearing when the soliton reaches the boundary; but this is probably of no importance for the test problem which emphasizes the initial evolution, before the soliton reaches the boundary. It is shown in [13] that the Neumann boundary conditions of common use, are better than the Dirichlet boundary conditions, but they still produce undesirable reflexions at the boundary which do not appear for the boundary conditions that we propose, based on the mathematical studies.

2. Part I: Multilevel methods for the shallow water equations

This Part is organized as follows. In Section 2.1 we present the shallow water system and the problem we are interested in: the solution of the system on a rectangular domain with either periodic boundary conditions or Dirichlet boundary conditions. In Section 2.2 we present the principle of the multilevel method. For the sake of simplicity, we present the method with two-levels of discretization, but the method can be easily extended to three and more levels. First we define the incremental unknowns, then we explain the multilevel algorithm and how the method can help to reduce the CPU time; then we describe the central-upwind finite volume scheme that we use. Section 2.3 deals with the space and time discretization of the shallow water equations using the central upwind scheme for the spatial discretization and a Runge–Kutta scheme of order 4 in time. In Section 2.4 we describe the results of the numerical simulations that we have done. We study in details in Section 2.4 the behavior of the method on an analytical test case corresponding to a known exact solution and show that it provides an accurate solution while reducing the CPU time.

2.1. Presentation of the problem

We apply finite volume multilevel scheme for the discretization of the nonlinear two-dimensional shallow water system on a rectangular domain $\mathcal{M} = (0, L_x) \times (0, L_y)$. This system is the following:

$$\begin{cases} \frac{\partial u\phi}{\partial t} + \frac{\partial \phi u^2}{\partial x} + \frac{\partial \phi uv}{\partial y} + \frac{g}{2} \frac{\partial \phi^2}{\partial x} = S_u, \\ \frac{\partial v\phi}{\partial t} + \frac{\partial \phi uv}{\partial x} + \frac{\partial \phi v^2}{\partial y} + \frac{g}{2} \frac{\partial \phi^2}{\partial y} = S_v, \\ \frac{\partial \phi}{\partial t} + \frac{\partial u\phi}{\partial x} + \frac{\partial v\phi}{\partial y} = S_\phi, \end{cases} \quad (1)$$

where ϕ is the fluid depth above the bottom, u and v are the x and y components of the velocity, and g denotes the gravity constant (see Fig. 1). All quantities are assumed nondimensional. We also denote $\mathbf{S} = (S_\phi, S_u, S_v)$ the source term which usually vanishes.

We write $u = u\phi$ and $v = v\phi$ (note the difference in fonts) and:

$$\mathbf{u} = \begin{pmatrix} u \\ v \\ \phi \end{pmatrix}, \quad F(\mathbf{u}) = \begin{pmatrix} \frac{u^2}{\phi} + \frac{g\phi^2}{2} \\ \frac{uv}{\phi} \\ u \end{pmatrix}, \quad G(\mathbf{u}) = \begin{pmatrix} \frac{uv}{\phi} \\ \frac{v^2}{\phi} + \frac{g\phi^2}{2} \\ v \end{pmatrix},$$

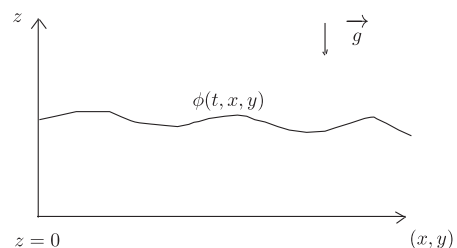


Fig. 1. Vertical section of the domain.

which allows us to write the system in the conservative form

$$\frac{\partial \mathbf{u}}{\partial t} + \frac{\partial F(\mathbf{u})}{\partial x} + \frac{\partial G(\mathbf{u})}{\partial y} = \mathbf{S}. \quad (2)$$

The discretization of \mathcal{M} is done using rectangular finite volumes $K_m = [x_{m/w}, x_{m/e}] \times [y_{m/s}, y_{m/n}]$ of centers (x_m, y_m) , (see Fig. 2), and of dimensions $\Delta x \times \Delta y$, with $N_x \Delta x = L_x$ and $N_y \Delta y = L_y$.

We use a NSWE (North–South–West–East) stencil which is presented in Fig. 3 to identify the unknowns.

The unknowns and the source terms will be approximations of the cell averages:

$$\mathbf{u}_m(t) = \frac{1}{\Delta x \Delta y} \int_{K_m} \mathbf{u}(x, y, t) dx dy,$$

where $\mathbf{u}_m(t) = (u_m(t), v_m(t), \phi_m(t))$ and,

$$\mathbf{S}_m(t) = \frac{1}{\Delta x \Delta y} \int_{K_m} \mathbf{S}(x, y, t) dx dy,$$

with $\mathbf{S}_m(t) = (S_{u_m}(t), S_{v_m}(t), S_{\phi_m}(t))$.

To derive the space discretized equations, we integrate the system (2) on each cell K_m , divide by its area $\Delta x \Delta y$, and we obtain:

$$\frac{d}{dt} \mathbf{u}_m(t) = - \frac{H_{m/e}^x(t) - H_{w/m}^x(t)}{\Delta x} - \frac{H_{m/n}^y(t) - H_{s/m}^y(t)}{\Delta y} + \mathbf{S}_m(t), \quad (3)$$

with \mathbf{S}_m representing the contribution of the source term.

Here $H_{m/e}^x(t)$ and $H_{m/n}^y(t)$, for example, are respectively the East flux (along the x axis) and the North flux (along the y axis) on the edges between K_m and K_e , and between K_m and K_n , and similarly for the other terms (see Fig. 2); for example:

$$H_{m/e}^x(t) = \frac{1}{\Delta x} \int_{\Gamma_{m/e}} F(\mathbf{u}(x, y, t)) dy$$

These fluxes depend on the method employed; we will consider central-upwind fluxes, which are made explicit in Section 2.3, see [35–38], but our multilevel method below can also be based on other fluxes.

2.2. Presentation of the multilevel method

The domain is discretized by two-levels of rectangular finite volume meshes: the fine mesh \mathcal{F}_1 counts $N_x \times N_y$ control volumes of dimensions $\Delta x \times \Delta y$, with $N_x \Delta x = L_x, N_y \Delta y = L_y$; and the coarse mesh \mathcal{F}_2 has $\frac{N_x N_y}{9}$ control volumes of dimensions $3\Delta x \times 3\Delta y$.

Here we use small letters for the fine mesh and capital letters for the coarse mesh: we denote by K_m a control volume of the fine mesh and by K_M a control volume of the coarse mesh (see Fig. 4).

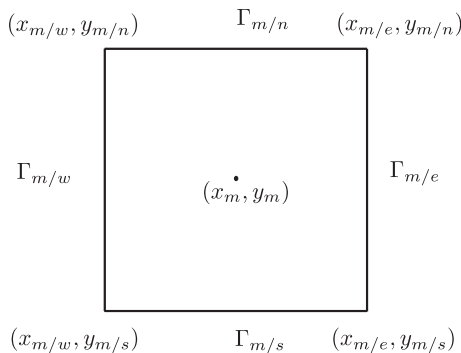


Fig. 2. A cell K_m .

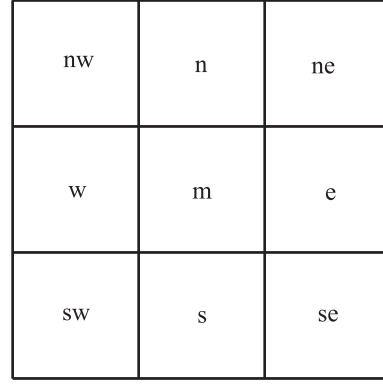


Fig. 3. The NSWE stencil.

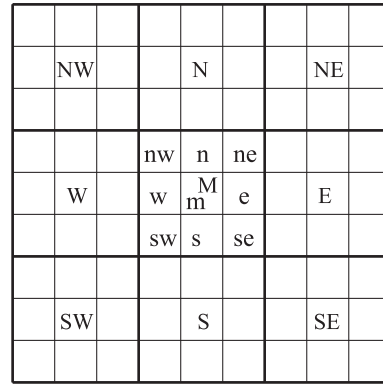


Fig. 4. The NSWE stencil with coarse and fine cells.

2.2.1. Incremental unknowns

We define the incremental unknowns for the conservative variables of the shallow water system, that is the three components of $\mathbf{u} = (u, v, \phi)$. We split each of the unknowns in a large-scale component $\mathbf{U} = (U, V, \Phi)$ and a small-scale component $\mathbf{Z} = (Z_u, Z_v, Z_\phi)$, which is meant to be frozen during a certain number of time steps. By large-scale and small-scale, we mean that \mathbf{U} contains the major information on the solution and that \mathbf{Z} represents a correcting term which is comparatively small, as explained in Lemma 3.1 below. For incremental unknowns defined by spectral decompositions like Fourier or wavelets, see [14–26,52,53].

Definition 1. Suppose that $\mathbf{u} = (u, v, \phi)$ is known on the fine mesh \mathcal{F}_1 . Then, on the control volume K_M , the large-scale component $\mathbf{U}_M = (U_M, V_M, \Phi_M)$ and the small-scale components $\mathbf{Z}_e, \mathbf{Z}_w, \mathbf{Z}_n, \mathbf{Z}_s, \mathbf{Z}_{ne}, \mathbf{Z}_{se}, \mathbf{Z}_{nw}, \mathbf{Z}_{sw}$ are defined as follows (see Fig. 5):

$$\begin{aligned} \mathbf{U}_M &= \frac{1}{9} (\mathbf{u}_m + \mathbf{u}_e + \mathbf{u}_w + \mathbf{u}_n + \mathbf{u}_s + \mathbf{u}_{ne} + \mathbf{u}_{nw} + \mathbf{u}_{se} + \mathbf{u}_{sw}), \\ \mathbf{Z}_e &= \mathbf{u}_e - \frac{1}{3} (\mathbf{U}_E + 2\mathbf{U}_M), \quad \mathbf{Z}_w = \mathbf{u}_w - \frac{1}{3} (\mathbf{U}_W + 2\mathbf{U}_M), \\ \mathbf{Z}_n &= \mathbf{u}_n - \frac{1}{3} (\mathbf{U}_N + 2\mathbf{U}_M), \quad \mathbf{Z}_s = \mathbf{u}_s - \frac{1}{3} (\mathbf{U}_S + 2\mathbf{U}_M), \\ \mathbf{Z}_{ne} &= \mathbf{u}_{ne} - \frac{1}{3} (\mathbf{U}_E + \mathbf{U}_M + \mathbf{U}_N), \quad \mathbf{Z}_{se} = \mathbf{u}_{se} - \frac{1}{3} (\mathbf{U}_S + \mathbf{U}_M + \mathbf{U}_E), \\ \mathbf{Z}_{nw} &= \mathbf{u}_{nw} - \frac{1}{3} (\mathbf{U}_W + \mathbf{U}_M + \mathbf{U}_N), \quad \mathbf{Z}_{sw} = \mathbf{u}_{sw} - \frac{1}{3} (\mathbf{U}_S + \mathbf{U}_M + \mathbf{U}_W), \end{aligned} \quad (4)$$

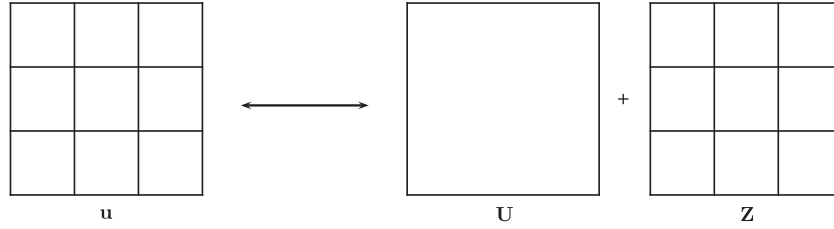


Fig. 5. The finite volume incremental unknowns.

Remark 1. The definition of the \mathbf{Z} in (4) is at our disposal. We chose them so that the \mathbf{Z} unknowns are of order $\Delta x^2 + \Delta y^2$ as stated and proven in Lemma 1.

Remark 2. Although all quantities are not used above and below, we have available on each coarse cell M and each fine cell m , the average values $\mathbf{u}_M, \mathbf{u}_m, S_M, S_m, \mathbf{U}_M, \mathbf{U}_m, \mathbf{Z}_M, \mathbf{Z}_m$.

Remark 3. Notice that the definition of the large-scale components \mathbf{U} differs from previous works on such incremental unknowns (see e.g. [29]). Indeed for the definition of the small-scale components in a coarse cell we use the values of the variable in the cell but also in the neighbor coarse cells, which is unusual. The large-scale component on a coarse cell K_M is defined by taking the mean value of the 9 fine-cell components of \mathbf{u} . Taking the mean on the 9 cells is crucial to ensure the numerical conservation of the scheme. We will discuss below the case of the boundary coarse cells when some of the needed neighboring coarse cells do not exist.

Remark 4. The correspondence between the solution on the fine mesh \mathbf{u} and its large-scale and small-scale components is one-to-one; that is knowing the component \mathbf{U} on the coarse mesh and the components \mathbf{Z} on the fine mesh, we can compute \mathbf{u} on the fine mesh; here are the recomposition formulas:

$$\begin{aligned} \mathbf{u}_m &= 5\mathbf{U}_M - \mathbf{U}_E - \mathbf{U}_W - \mathbf{U}_N - \mathbf{U}_S - (\mathbf{Z}_e + \mathbf{Z}_w + \mathbf{Z}_n + \mathbf{Z}_s + \mathbf{Z}_{ne} \\ &\quad + \mathbf{Z}_{se} + \mathbf{Z}_{nw} + \mathbf{Z}_{sw}), \\ \mathbf{u}_e &= \mathbf{Z}_e + \frac{1}{3}(\mathbf{U}_E + 2\mathbf{U}_M), \quad \mathbf{u}_w = \mathbf{Z}_w + \frac{1}{3}(\mathbf{U}_W + 2\mathbf{U}_M), \\ \mathbf{u}_n &= \mathbf{Z}_n + \frac{1}{3}(\mathbf{U}_N + 2\mathbf{U}_M), \quad \mathbf{u}_s = \mathbf{Z}_s + \frac{1}{3}(\mathbf{U}_S + 2\mathbf{U}_M), \\ \mathbf{u}_{ne} &= \mathbf{Z}_{ne} + \frac{1}{3}(\mathbf{U}_E + \mathbf{U}_M + \mathbf{U}_N), \quad \mathbf{u}_{se} = \mathbf{Z}_{se} + \frac{1}{3}(\mathbf{U}_S + \mathbf{U}_M + \mathbf{U}_E), \\ \mathbf{u}_{nw} &= \mathbf{Z}_{nw} + \frac{1}{3}(\mathbf{U}_W + \mathbf{U}_M + \mathbf{U}_N), \quad \mathbf{u}_{sw} = \mathbf{Z}_{sw} + \frac{1}{3}(\mathbf{U}_S + \mathbf{U}_M + \mathbf{U}_W). \end{aligned}$$

Remark 5. It is important to observe that this definition of the incremental unknowns is recursive: once the \mathbf{U} and \mathbf{Z} corresponding to the second level coarse grid have been calculated, we can split \mathbf{U} by the same means to find the \mathbf{U} and \mathbf{Z} corresponding to a finer level of discretization, that is to say the \mathbf{U} of the second level plays then the role of the large-scale variable for the third level.

Using Taylor's formula, we can show that the small-scale components \mathbf{Z} are small compared to the large-scale components, which are of the same order as \mathbf{u} :

Lemma 1. The small-scale components $\mathbf{Z}_e, \mathbf{Z}_w, \mathbf{Z}_s, \mathbf{Z}_n, \mathbf{Z}_{ne}, \mathbf{Z}_{se}, \mathbf{Z}_{nw}, \mathbf{Z}_{sw}$ are of order $\Delta x^2 + \Delta y^2$.

Proof. Using Taylor's formula, we have indeed for \mathbf{Z}_s for example:

$$\begin{aligned} \mathbf{Z}_s &= \mathbf{u}_s - \frac{1}{3}(\mathbf{U}_S + 2\mathbf{U}_M) \\ &= \mathbf{u}_s - \frac{1}{27}[\mathbf{u}_{Sm} + \mathbf{u}_{Se} + \mathbf{u}_{Sw} + \mathbf{u}_{Sn} + \mathbf{u}_{Ss} + \mathbf{u}_{Sne} + \mathbf{u}_{Snw} + \mathbf{u}_{Sse} \\ &\quad + \mathbf{u}_{Ssw} + 2(\mathbf{u}_m + \mathbf{u}_e + \mathbf{u}_w + \mathbf{u}_n + \mathbf{u}_s + \mathbf{u}_{ne} + \mathbf{u}_{nw} + \mathbf{u}_{se} + \mathbf{u}_{sw})] \\ &= \frac{1}{27}[25\mathbf{u}_s - (\mathbf{u}_s - 2\Delta y\partial_y\mathbf{u}_s) - (\mathbf{u}_s - \Delta x\partial_x\mathbf{u}_s - 2\Delta y\partial_y\mathbf{u}_s) \\ &\quad - (\mathbf{u}_s + \Delta x\partial_x\mathbf{u}_s - 2\Delta y\partial_y\mathbf{u}_s) - (\mathbf{u}_s - \Delta y\partial_y\mathbf{u}_s) - (\mathbf{u}_s - 3\Delta y\partial_y\mathbf{u}_s) \\ &\quad - (\mathbf{u}_s - \Delta x\partial_x\mathbf{u}_s - \Delta y\partial_y\mathbf{u}_s) - (\mathbf{u}_s + \Delta x\partial_x\mathbf{u}_s - \Delta y\partial_y\mathbf{u}_s) \\ &\quad - (\mathbf{u}_s - \Delta x\partial_x\mathbf{u}_s - 3\Delta y\partial_y\mathbf{u}_s) - (\mathbf{u}_s + \Delta x\partial_x\mathbf{u}_s - 3\Delta y\partial_y\mathbf{u}_s) \\ &\quad - 2(\mathbf{u}_s + \Delta y\partial_y\mathbf{u}_s) - 2(\mathbf{u}_s + 2\Delta y\partial_y\mathbf{u}_s) - 2(\mathbf{u}_s + \Delta x\partial_x\mathbf{u}_s + \Delta y\partial_y\mathbf{u}_s) \\ &\quad - 2(\mathbf{u}_s - \Delta x\partial_x\mathbf{u}_s + \Delta y\partial_y\mathbf{u}_s) - 2(\mathbf{u}_s + \Delta x\partial_x\mathbf{u}_s) - 2(\mathbf{u}_s + 2\Delta x\partial_x\mathbf{u}_s) \\ &\quad - 2(\mathbf{u}_s - \Delta x\partial_x\mathbf{u}_s + 2\Delta y\partial_y\mathbf{u}_s) - 2(\mathbf{u}_s + \Delta x\partial_x\mathbf{u}_s + 2\Delta y\partial_y\mathbf{u}_s)] \\ &\quad + \mathcal{O}(\Delta x^2 + \Delta y^2). \end{aligned}$$

We observe that the expression between brackets after $1/27$ actually vanishes so that finally:

$$\mathbf{Z}_s = \mathcal{O}(\Delta x^2 + \Delta y^2).$$

It works similarly for $\mathbf{Z}_e, \mathbf{Z}_w, \mathbf{Z}_n, \mathbf{Z}_{ne}, \mathbf{Z}_{se}, \mathbf{Z}_{sw}, \mathbf{Z}_{nw}$. \square

2.2.2. The multilevel scheme

2.2.2.1. Scheme on the coarse grid. We split each component of $\mathbf{u} = (u, v, \phi)$ into its large-scale component $\mathbf{U} = (U, V, \Phi)$ and its small-scale component (Z_u, Z_v, Z_ϕ) . To obtain the scheme on the coarse grid of level 2, we write (9.1) on each fine cell $K_m, K_e, K_w, K_n, K_s, K_{ne}, K_{se}, K_{nw}, K_{sw}$ of the coarse cell K_M (see Fig. 4), and we take the mean value by summing all these equations and dividing by 9. This results in:

$$\begin{aligned} \frac{d}{dt}\mathbf{U}_M(t) &= \frac{1}{9\Delta x} \left[H_{m/w}^x - H_{m/e}^x + H_{n/nw}^x - H_{n/ne}^x + H_{s/sw}^x - H_{s/se}^x \right. \\ &\quad + H_{w/w}^x - H_{m/w}^x + H_{nw/Wne}^x - H_{nw/n}^x + H_{sw/Wse}^x - H_{sw/s}^x \\ &\quad + H_{n/ne}^x - H_{Enw/ne}^x + H_{m/e}^x - H_{e/Ew}^x - H_{se/Esw}^x + H_{s/se}^x \left. \right] \\ &\quad + \frac{1}{9\Delta y} \left[H_{m/n}^y - H_{n/Ns}^y + H_{s/m}^y - H_{n/m}^y + H_{s/Sn}^y - H_{s/m}^y \right. \\ &\quad + H_{ne/e}^y - H_{ne/Nse}^y + H_{e/se}^y - H_{ne/e}^y + H_{se/Snw}^y - H_{se/e}^y + H_{nw/w}^y \\ &\quad \left. - H_{nw/Nsw}^y + H_{sw/w}^y - H_{w/nw}^y + H_{sw/Sne}^y - H_{sw/w}^y \right] + \mathbf{S}_M(t), \quad (5) \end{aligned}$$

with:

$$\begin{aligned} \mathbf{S}_M(t) &= \frac{1}{9}(\mathbf{S}_{nw}(t) + \mathbf{S}_n(t) + \mathbf{S}_{ne}(t) + \mathbf{S}_w(t) + \mathbf{S}_n(t) + \mathbf{S}_e(t) \\ &\quad + \mathbf{S}_{sw}(t) + \mathbf{S}_s(t) + \mathbf{S}_{se}(t)). \quad (6) \end{aligned}$$

In (5) the definition of the fluxes such as $H_{m/w}^x, H_{m/nw}^x$ is obvious and the less obvious fluxes such as $H_{w/w}^x$ relate to the edges shown in Fig. 6. Eq. (5) gives after simplifications the following semi-discrete scheme to be applied on the coarse grid of level 2:

$$\begin{aligned} \frac{d}{dt} \mathbf{U}_M(t) = & \frac{1}{9\Delta x} \left[(H_{nw/Wne}^x + H_{We/w}^x + H_{sw/Wse}^x) \right. \\ & \left. - (H_{Enw/ne}^x + H_{e/Ew}^x + H_{se/Esw}^x) \right] + \frac{1}{9\Delta y} \left[(H_{sw/Sne}^y + H_{s/Sn}^y + H_{se/Snw}^y) \right. \\ & \left. - (H_{nw/Nsw}^y + H_{n/Ns}^y + H_{ne/Nse}^y) \right] + \mathbf{S}_M(t). \end{aligned} \quad (7)$$

Remark 6. Note that formula (7) corresponds just to the averaging of Eqs. (3) on the 9 cells corresponding to the coarse cell M. Of course this process is completely recursive and can be repeated for simulations on three or more levels of grids.

We can now conceive different numerical schemes depending on the definition (choice) of the fluxes and the solution on the coarse level can be done locally in certain parts of the domain. We ought also to choose the time discretization for $d\mathbf{U}_M/dt$. Concerning the spatial discretization we chose to freeze the \mathbf{Z} components during the iterations on the coarse grid, while the large-scale components \mathbf{U} are computed through this scheme.

2.2.2.2. Multilevel algorithm. The small-scale components \mathbf{Z} have an important effect on the size of the error. To explain this, let us describe the multilevel algorithm in details.

For a general multilevel situation, let us fix the number N_{max} of levels of grids on which we are going to compute. From $t = 0$ until the final time T , we repeat N_{it}/L times (where N_{it} is the total number of iterations) the cycle $n_1 n_2 \dots n_L$ where for $1 \leq i \leq L$, n_i stands for an iteration on the level n_i , $1 \leq n_i \leq N_{max}$. For example for a simulation on two-levels, as considered here, we chose to repeat cycles of the form: 111122221111, where 1 corresponds to the fine grid and 2 to the coarse one. Of course alternate choices of the sequence of levels are possible and, in future work, we intend to develop adaptative procedures for changing the levels. Therefore at the n th iteration, we compute:

- At level 1 we work on the fine mesh \mathcal{F}_1 and compute \mathbf{u}^{n+1} with the classical scheme (described in our case in (9) and (10) below).
- At level 2
 - we calculate explicitly the fluxes needed by the scheme (7),
 - we split \mathbf{u}^n into its large-scale \mathbf{U}^n and small-scale \mathbf{Z}^n components,
 - we compute \mathbf{U}^{n+1} with (7),
 - we recompose \mathbf{u}^{n+1} from \mathbf{U}^{n+1} and \mathbf{Z}^n .

We freeze the small-scale components \mathbf{Z} during each iteration at level 2. This induces an error on \mathbf{Z} of the order $\Delta t \times$ magnitude of $\mathbf{Z} = \Delta t(\Delta x^2 + \Delta y^2)$. This error committed in freezing \mathbf{Z} adds up

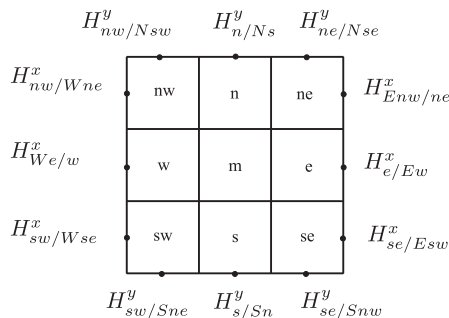


Fig. 6. Fluxes needed for an iteration of the scheme on the coarse grid to calculate \mathbf{y}^{n+1} on K_M .

to the classical error (see Section 2.4); this time variation thus needs to be controlled during the simulations.

2.2.2.3. Gain of CPU time. It is important to notice that implementing the scheme on the coarse grid requires to calculate the fluxes on the fine grid only on the exterior edges of the coarse cell, as indicated in Fig. 6.

When implementing such schemes in the context of shallow water equations, the most time consuming step during one iteration is the calculation of the fluxes; therefore the multilevel method is expected to reduce significantly the CPU time.

Indeed, if we implement the classical finite volume scheme using it only on one-level namely the fine mesh \mathcal{F}_1 which has $N_x \times N_y$ control volumes, for each time iteration, we need to calculate the fluxes on $2N_x N_y + N_x + N_y$ edges.

Now with the multilevel method implemented on two-levels of grids \mathcal{M}_1 and \mathcal{M}_2 , during an iteration on the coarse grid, the fluxes need to be evaluated on $2N_x N_y/3 + N_x + N_y$ edges. This means that for this iteration, we gain \mathcal{G} computations of fluxes, where

$$\mathcal{G} = \frac{4N_x N_y}{3}.$$

In the particular case of a square mesh (that we will consider in the numerical experiments),

$$\mathcal{G} = 4N_x^2/3,$$

and this corresponds to a computational saving of

$$\left(100 \times \frac{2}{3} \frac{N_x}{N_x + 1} \right) \%.$$

For example if we work on two-levels with two grids of 300×300 and 100×100 , this means a gain of 66.4% for each iteration on the coarse grid. We notice that the maximum gain in percentage that we can expect is less than 66.66%, and that when the number of cells of the fine mesh ($N_x \times N_y$) increases, the gain gets closer to this maximal value.

The behavior of the multilevel method then depends on the number of iterations performed on the coarse level: as this number increases, the CPU-time decreases, whereas the error increases. Nevertheless, in order to be sure that we obtain a good approximation of the solution, we need to check that the error when using the multilevel method ranges between the error made when calculating on the fine level and that made when calculating on the coarse level and this appears clearly in Fig. 13. This will ensure that the multilevel method enables us to get a better solution than when calculating on the coarse level, while being faster than the classical one-level method on the fine grid. We have to make a compromise between these two aspects. In our case we obtained a gain of 15.6% of CPU time for a given accuracy.

2.3. The multilevel method with central-upwind schemes

2.3.1. Spatial discretization

The space discretization is done using a semi-discrete central-upwind scheme (as in [37,38]); we describe here in detail the expression of these central-upwind fluxes. These types of schemes have the advantage of being perfectly adapted to the discretization of hyperbolic systems of conservation laws due to their upwind nature while being robust and simple since they do not require to solve any Riemann problem; moreover they are nonstaggered schemes. The starting point of the construction of this type of schemes is the equivalent integral formulation of the system. They are based on integration over Riemann fans using the one-sided local speeds of propagation.

Recall that the semi-discrete form of the scheme reads:

$$\frac{d}{dt} \mathbf{u}_m(t) = -\frac{H_{m/e}^x(t) - H_{w/m}^x(t)}{\Delta x} - \frac{H_{m/n}^y(t) - H_{s/m}^y(t)}{\Delta y} + \mathbf{S}_m(t). \quad (8)$$

Eq. (8) is exact. The approximation procedure starts with the approximation definitions of the fluxes that we choose. We first use a second order version following [37,38], and the corresponding numerical fluxes are:

$$H_{m/e}^x \cong \frac{a_{m/e}^+ F(\mathbf{u}_m^E) - a_{m/e}^- F(\mathbf{u}_e^W)}{a_{m/e}^+ - a_{m/e}^-} + \frac{a_{m/n}^+ a_{m/e}^- (\mathbf{u}_e^W - \mathbf{u}_m^E)}{a_{m/e}^+ - a_{m/e}^-} \quad (9)$$

and

$$H_{m/n}^y \cong \frac{b_{m/n}^+ G(\mathbf{u}_m^N) - b_{m/n}^- G(\mathbf{u}_n^S)}{b_{m/n}^+ - b_{m/n}^-} + \frac{b_{m/n}^+ b_{m/n}^- (\mathbf{u}_n^S - \mathbf{u}_m^N)}{b_{m/n}^+ - b_{m/n}^-}. \quad (10)$$

With F, G as in (2), we use a non-oscillatory linear polynomial reconstruction to evaluate the following point values which are present in (9) and (10):

$$\mathbf{u}_m^E = \zeta_m(x_{m/e}, y_m, t), \quad \mathbf{u}_m^W = \zeta_m(x_{m/w}, y_m, t),$$

$$\mathbf{u}_m^N = \zeta_m(x_m, y_{m/n}, t), \quad \mathbf{u}_m^S = \zeta_m(x_m, y_{m/s}, t).$$

where $\zeta_m(x_m, y_m, t) = \mathbf{u}_m(t) + s_m^x(t)(x - x_m) + s_m^y(t)(y - y_m)$.

We use a piecewise linear reconstruction in order to obtain a second order scheme. The order of the scheme also relates to the order of the quadrature formula used to approximate the flux integrals coming from the integral formulation.

The slopes of this linear approximation are calculated using a minmod limiter:

$$s_m^x(t) = \text{minmod}\left(\theta \frac{\mathbf{u}_m(t) - \mathbf{u}_w(t)}{\Delta x}; \frac{\mathbf{u}_e(t) - \mathbf{u}_w(t)}{2\Delta x}; \theta \frac{\mathbf{u}_e(t) - \mathbf{u}_m(t)}{\Delta x}\right),$$

$$s_m^y(t) = \text{minmod}\left(\theta \frac{\mathbf{u}_m(t) - \mathbf{u}_s(t)}{\Delta y}; \frac{\mathbf{u}_n(t) - \mathbf{u}_s(t)}{2\Delta y}; \theta \frac{\mathbf{u}_n(t) - \mathbf{u}_m(t)}{\Delta y}\right), \quad (11)$$

where minmod of a vector is understood by components and for scalar arguments it is defined by:

$$\text{minmod}(x_1, x_2, \dots) := \begin{cases} \min(x_i), & \text{if } x_i > 0 \forall i \\ \max(x_i), & \text{if } x_i < 0 \forall i \\ 0, & \text{otherwise.} \end{cases}$$

where $\theta \in [1, 2]$.

An appropriate choice of these approximate derivatives is crucial to ensure that the above reconstruction is nonoscillatory in the sense of preventing appearance of new extrema in the solution; it can be shown that with such approximate derivatives the scheme satisfies the scalar total-variation-diminishing (TVD) property (see [35,37]). The parameter $\theta \in [1, 2]$ has to be chosen in an empirical optimal way in order to obtain good results.

The one-sided local speeds of propagation are given by:

$$a_{m/e}^+ = \max \left[\lambda_{\max} \left(\frac{\partial F}{\partial \mathbf{u}}(\mathbf{u}_e^W) \right), \lambda_{\max} \left(\frac{\partial F}{\partial \mathbf{u}}(\mathbf{u}_m^E) \right), 0 \right],$$

$$a_{m/e}^- = \min \left[\lambda_{\min} \left(\frac{\partial F}{\partial \mathbf{u}}(\mathbf{u}_e^W) \right), \lambda_{\min} \left(\frac{\partial F}{\partial \mathbf{u}}(\mathbf{u}_m^E) \right), 0 \right], \quad (12)$$

$$b_{m/n}^+ = \max \left[\lambda_{\max} \left(\frac{\partial G}{\partial \mathbf{u}}(\mathbf{u}_n^S) \right), \lambda_{\max} \left(\frac{\partial G}{\partial \mathbf{u}}(\mathbf{u}_m^N) \right), 0 \right],$$

$$b_{m/n}^- = \min \left[\lambda_{\min} \left(\frac{\partial G}{\partial \mathbf{u}}(\mathbf{u}_n^S) \right), \lambda_{\min} \left(\frac{\partial G}{\partial \mathbf{u}}(\mathbf{u}_m^N) \right), 0 \right],$$

where $\lambda_{\max}(\frac{\partial F}{\partial \mathbf{u}}(\tilde{\mathbf{u}}))$ and $\lambda_{\min}(\frac{\partial F}{\partial \mathbf{u}}(\tilde{\mathbf{u}}))$ (resp. $\lambda_{\max}(\frac{\partial G}{\partial \mathbf{u}}(\tilde{\mathbf{u}}))$ and $\lambda_{\min}(\frac{\partial G}{\partial \mathbf{u}}(\tilde{\mathbf{u}}))$) are respectively the largest and the smallest eigenvalue of the Jacobian matrix of $F, \frac{\partial F}{\partial \mathbf{u}}$ (resp. of $G, \frac{\partial G}{\partial \mathbf{u}}$) at the point $\tilde{\mathbf{u}}$.

Remark 7. The terminology ‘‘central-upwind’’ introduced in Kurganov et al. [37], is justified as follows: the finite differences quotients used in the right hand side of (10) correspond to central finite differences that is e.g. $\frac{\partial u}{\partial x}|_m$ is somehow approximated by $\frac{1}{\Delta x}(u_{|m/e} - u_{|w/m})$. However the values $u_{|m/e}, u_{|w/m}$ are replaced by the fluxes $H_{m/e}^x$ and $H_{w/m}^x$ and the fluxes defined in (9)–(11) take into account the direction of the flow through the coefficients a^+, a^-, b^+, b^- , as defined in (12). This gives us a central-upwind scheme of second order.

Boundary conditions with central-upwind schemes. When we consider periodic boundary conditions, then the quantities on the boundaries are evaluated using periodicity.

2.3.2. Time discretization with Runge–Kutta method

For the time discretization, we use a fourth order Runge–Kutta method. Let $T > 0$ be fixed, denote the time step by $\Delta t = T/N_{it}$, where N_{it} is an integer representing the total number of time iterations; for $n = 0, \dots, N_{it}$ we define \mathbf{u}^n as the approximate value of \mathbf{u} at time $t_n = n\Delta t$.

We rewrite (3) as

$$\frac{d}{dt} \mathbf{u}_m = R(\mathbf{u}_m(t), t),$$

and apply the following time discretization:

$$\begin{cases} k_{1,m}^n = R(\mathbf{u}_m^n, t_n), \\ k_{2,m}^n = R(\mathbf{u}_m^n + \frac{\Delta t}{2} k_{1,m}^n, t_n + \frac{\Delta t}{2}), \\ k_{3,m}^n = R(\mathbf{u}_m^n + \frac{\Delta t}{2} k_{2,m}^n, t_n + \frac{\Delta t}{2}), \\ k_{4,m}^n = R(\mathbf{u}_m^n + \Delta t k_{3,m}^n, t_n + \Delta t), \\ \mathbf{u}_m^{n+1} = \mathbf{u}_m^n + \frac{\Delta t}{6} (k_{1,m}^n + 2k_{2,m}^n + 2k_{3,m}^n + k_{4,m}^n). \end{cases} \quad (13)$$

2.4. Numerical simulations

We present here the numerical results obtained by using the multilevel method that we just described.

We consider a square domain $\mathcal{M} = (0, L) \times (0, L)$ with periodic boundary conditions. In order to study the performance of the multilevel scheme, we first consider analytical solutions; we solve the non-dimensional shallow water system with the initial conditions:

$$\begin{pmatrix} u \\ v \\ \phi \end{pmatrix} = \begin{pmatrix} u(x, y, 0) \\ v(x, y, 0) \\ \phi(x, y, 0) \end{pmatrix},$$

these values being taken from (14) below and we also compute with the source terms so that

$$u(x, y, t) = u_0 \left(1 + \epsilon \sin \left(\frac{2\pi t}{T} \right) \cos \left(\frac{4\pi x}{L} \right) \cos \left(\frac{4\pi y}{L} \right) \right),$$

$$v(x, y, t) = u_0 \left(1 + \epsilon \sin \left(\frac{2\pi t}{T} \right) \sin \left(\frac{4\pi x}{L} \right) \cos \left(\frac{4\pi y}{L} \right) \right), \quad (14)$$

$$\phi(x, y, t) = \phi_0 \left(1 + \epsilon \sin \left(\frac{2\pi t}{T} \right) \cos \left(\frac{4\pi x}{L} \right) \sin \left(\frac{4\pi y}{L} \right) \right),$$

is the exact solution of the system to which we can compare the computed solution.

Here we take $L = 10$ km; the average height and speed of the fluid are respectively $\phi_0 = 1$ km and $u_0 = 0.1$ km/s, and ϵ measures the amplitude of the wave, here $\epsilon = 0.2$. The time period of the exact solution is $T = 0.5$ s and the time step retained for all the computations is $\Delta t = 10^{-4}$ s. Let us introduce the small nondimensional parameter $\mu = (\phi_0/L)^2$ which measures the shallowness of the flow; here $\mu = 10^{-2}$ and the Stokes number which compares the dispersive effects and the nonlinear effects is $S = \epsilon/\mu = 20$. We are thus indeed in the framework of a shallow water flow (large amplitude

and shallowness), which renders the flow *strongly nonlinear*. The nondimensional parameter θ in (11) is taken to be $\theta = 1.6$ and the fine mesh \mathcal{M}_1 counts 90,000 cells which corresponds to a space step equal to $\Delta x = \Delta y = 10/300 \text{ km} \approx 33.33 \text{ m}$.

First, we make a one-level computation on the fine mesh \mathcal{M}_1 in order to study the behavior of the small-scale and of the large-scale components \mathbf{Z} and \mathbf{U} of the conservative variables corresponding to the coarser level of discretization which here is level two. We plot the time evolution of the discrete norms of the following quantities for:

$$\|\mathbf{u}^n\|_2 = \sqrt{\sum_{K_m \in \mathcal{M}_1} \Delta x \Delta y |\mathbf{u}_m^n|^2},$$

$$\|\mathbf{U}^n\|_2 = \sqrt{\sum_{K_M \in \mathcal{M}_2} 9 \Delta x \Delta y |\mathbf{U}_M^n|^2},$$

$$\|\mathbf{Z}^n\|_2 = \sqrt{\sum_{K_m \in \mathcal{M}_1} \Delta x \Delta y |\mathbf{Z}_m^n|^2},$$

where \mathcal{M}_2 denotes the coarse mesh, and similarly for u and v ; above and below $|\cdot|$ stands for the Euclidian norm in \mathbb{R}^3 . We also plot the time evolution of their variations

$$\|d\mathbf{u}^n\|_2 = \sqrt{\sum_{K_m \in \mathcal{M}_1} \Delta x \Delta y |\mathbf{u}_m^n - \mathbf{u}_m^{n-1}|^2},$$

$$\|d\mathbf{U}^n\|_2 = \sqrt{\sum_{K_M \in \mathcal{M}_2} 9 \Delta x \Delta y |\mathbf{U}_M^n - \mathbf{U}_M^{n-1}|^2}, \quad (15)$$

$$\|d\mathbf{Z}^n\|_2 = \sqrt{\sum_{K_m \in \mathcal{M}_1} \Delta x \Delta y |\mathbf{Z}_m^n - \mathbf{Z}_m^{n-1}|^2}.$$

The graphs that we obtain are presented in Figs. 7 and 8. As expected, the norms of ϕ , u and v are respectively of the same order as the norms of Φ , U , V , and the norms of Z_ϕ , Z_u , and Z_v are small in accordance with Lemma 1. Moreover Figs. 7 and 8 show that the time variation of the large-scale components \mathbf{U} of the conservative variables ϕ , u , and v are similar to the variation of ϕ , u , and v and the time variation of the small-scale components \mathbf{Z} satisfy $\|d\mathbf{Z}\|_2 = \mathcal{O}(\Delta t^{3/2})^1$; the order of magnitude of this norm is crucial for the efficiency of the multilevel method. Indeed during an iteration on the coarse grid, the \mathbf{Z} 's are frozen, which means that $\mathbf{Z}^{n+1} = \mathbf{Z}^n$. But normally,

$$\mathbf{Z}^{n+1} - \mathbf{Z}^n = \Delta t \frac{\partial \mathbf{Z}}{\partial t} + \mathcal{O}(\Delta t^2),$$

that is $\mathbf{Z}^{n+1} = \mathbf{Z}^n + \delta$ where $\delta = \Delta t \frac{\partial \mathbf{Z}}{\partial t} + \mathcal{O}(\Delta t^2)$.

Consequently, if $\frac{\partial \mathbf{Z}}{\partial t} = \mathcal{O}(\Delta t)$ then $\delta = \mathcal{O}(\Delta t^2)$ and freezing the \mathbf{Z} is legitimate, whereas $\mathbf{Z}^{n+1} - \mathbf{Z}^n = \mathcal{O}(\Delta t)$ means that $\delta = \Delta t \frac{\partial \mathbf{Z}}{\partial t} = \mathcal{O}(\Delta t)$ or $\frac{\partial \mathbf{Z}}{\partial t} = \mathcal{O}(1)$ and freezing the \mathbf{z}^n introduces significant errors.

The quantity $\frac{\partial \mathbf{Z}}{\partial t}$ can be computed explicitly and is linked to the space step. Indeed, we find, using Taylor's formula, that

$$\mathbf{z}_e = -\frac{4}{3} \Delta x^2 \frac{\partial^2 \mathbf{u}_e}{\partial x^2} - \frac{1}{3} \Delta y^2 \frac{\partial^2 \mathbf{u}_e}{\partial y^2},$$

$$\mathbf{z}_{ne} = -\frac{4}{3} \Delta x^2 \frac{\partial^2 \mathbf{u}_e}{\partial x^2} - \frac{4}{3} \Delta y^2 \frac{\partial^2 \mathbf{u}_e}{\partial y^2} - \Delta x \Delta y \frac{\partial^2 \mathbf{u}_e}{\partial x \partial y},$$

and

$$\frac{\partial \mathbf{z}_e}{\partial t} = -\frac{4}{3} \Delta x^2 \frac{\partial^3 \mathbf{u}_e}{\partial t \partial x^2} - \frac{1}{3} \Delta y^2 \frac{\partial^3 \mathbf{u}_e}{\partial t \partial y^2},$$

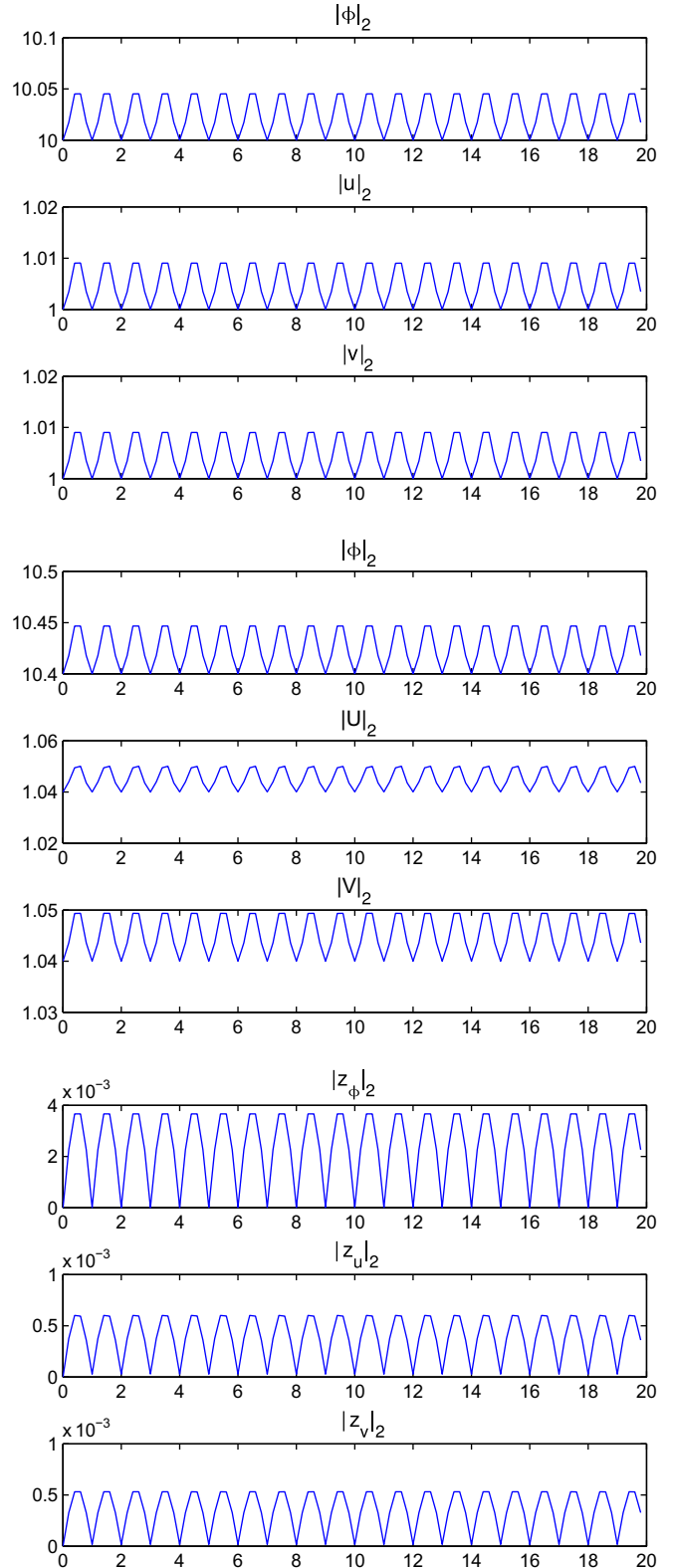


Fig. 7. Time evolution of the discrete L^2 -norms of the conservative variables.

$$\frac{\partial \mathbf{z}_{ne}}{\partial t} = -\frac{4}{3} \Delta x^2 \frac{\partial^3 \mathbf{u}_e}{\partial t \partial x^2} - \frac{4}{3} \Delta y^2 \frac{\partial^3 \mathbf{u}_e}{\partial t \partial y^2} - \Delta x \Delta y \frac{\partial^3 \mathbf{u}_e}{\partial t \partial x \partial y},$$

and similarly for the other \mathbf{Z} terms. In a future work, this quantity could be used as a criterion to selectively decide whether a way down on the coarse level is reasonable in order to control the de-

¹ $\mathcal{O}(\Delta t^m)$ means $\leq C \Delta t^m$, where C is a constant of macroscopic scale for the corresponding physical quantity.

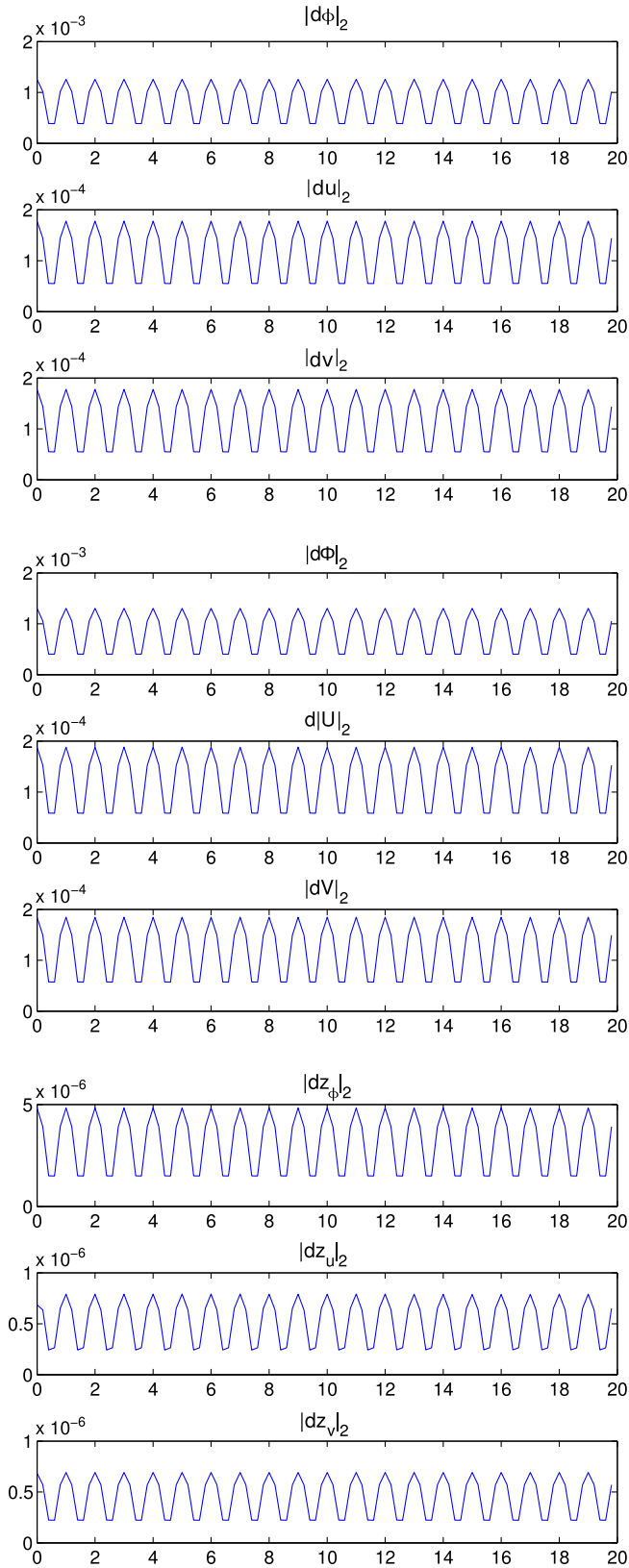


Fig. 8. Time evolution of the discrete L^2 -norms of the variations of the conservative variables as defined in (15).

cents from the fine grid levels to the coarse level and the ascents from a coarse level to a finer level instead of following systematic cycles as is done in the simulations presented here (cycle of 1111122222211111).

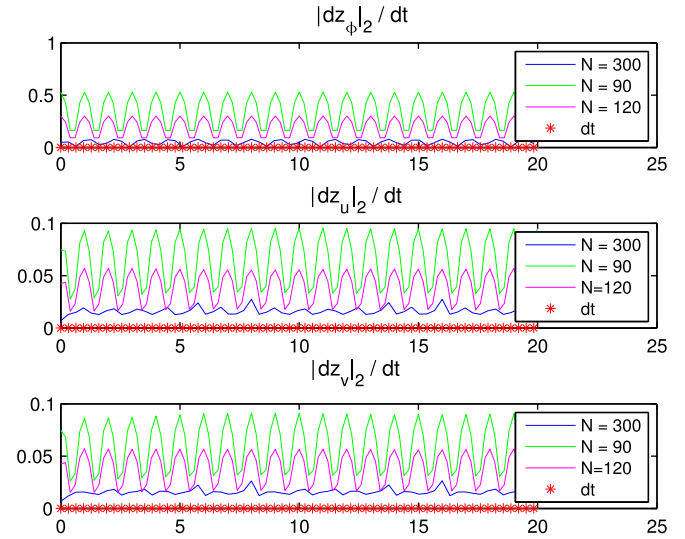


Fig. 9. Time evolution of the L^2 -norms of the variations of the variables with different space steps.

For the test case that we study, the order of magnitude of $\frac{\partial \mathbf{z}^n}{\partial t}$ can thus be evaluated and we find values which agree with the curves presented in Fig. 8. To show the importance of the space step we repeat several computations on different fine meshes (with 90×90 and 120×120 control volumes) and plot in Fig. 9 the evolution of $\frac{\mathbf{z}^{n+1} - \mathbf{z}^n}{\Delta t}$ which is compared to Δt . The multilevel method with 300×300 cells is expected to work well up to a certain point since $\frac{\partial \mathbf{z}^n}{\partial t}$ is not too far from $\mathcal{O}(\Delta t)$; of course the larger the space step is, the larger the value of $\frac{\partial \mathbf{z}^n}{\partial t}$ will be and the less accurate the multilevel method will be. The multilevel computation with the mesh using 120×120 control volumes is still more precise than the computation on the coarse grid, but with 90×90 cells, $\frac{\partial \mathbf{z}^n}{\partial t}$ is much larger than Δt and the multilevel method provides too large errors: the errors obtained are too close from the ones obtained with a computation on the coarse grid, for the multilevel method to be profitable (see Fig. 10).

Consequently the multilevel method is expected to work better for a smaller space step; and it enables to descend on coarser levels and to spend more iterations on the coarser levels, which provides a more important gain in CPU time while preserving the accuracy of the solution.

In a second step we use the multilevel method to solve the same problem with two-levels of discretization. The coarse mesh \mathcal{M}_2 counts 100×100 cells with a space step $\Delta x = 0.1$. This computation is made by beginning with a few iterations on the fine mesh, and then repeating cycles of the form 111112222211111 where 1 corresponds to the fine level and 2 to the coarse one, which means that we perform about 37.5% of the iterations on the coarse grid (see Fig. 15); in the following, we refer to this simulation as the multilevel method at 37% (MM37).

We show in Fig. 11 the solutions obtained at $t = 20$ with the multilevel method on the right, which are visually very similar to the reference solutions obtained with the one-level computation on the fine mesh and depicted on the left of the figure (which is very similar to the exact solution available in this example). For more readability we also represent the differences between the multilevel solutions and the reference solutions on Fig. 12; they are small and agree with the errors obtained.

Notice that the reconstruction of the solution at each iteration with the frozen small-scale component \mathbf{Z} leads to the appearance of very small peaks on the solution; a zoom on the solution is necessary to see them. Indeed, suppose that the large-scale component \mathbf{U}^n of \mathbf{u} at the n th iteration is exact and suppose that the

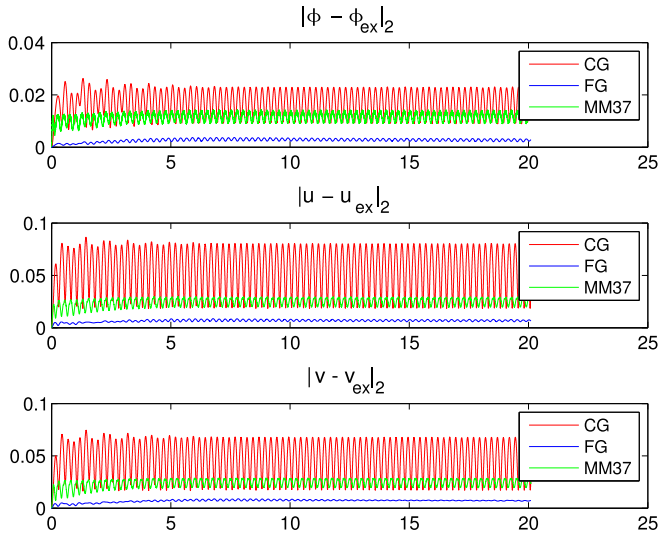


Fig. 10. Time evolution of the L^2 errors obtained with a multilevel computation at 37% and with a computation on the fine grid for a mesh of 90×90 cells.

variation of the \mathbf{Z} during this iteration is of order η , namely $\mathbf{Z}^n = \mathbf{Z}^{n-1} + \eta$. After an iteration on the coarse grid, we recompute the solution with \mathbf{Z}^{n-1} by freezing the small-scale component and find:

$$\begin{aligned} \mathbf{u}_m^n &= 5\mathbf{U}_M^n - \mathbf{U}_E^n - \mathbf{U}_W^n - \mathbf{U}_S^n - \mathbf{U}_N^n - \mathbf{Z}_e^{n-1} - \mathbf{Z}_w^{n-1} - \mathbf{Z}_s^{n-1} - \mathbf{Z}_n^{n-1} - \mathbf{Z}_{ne}^{n-1} \\ &\quad - \mathbf{Z}_{nw}^{n-1} - \mathbf{Z}_{se}^{n-1} - \mathbf{Z}_{sw}^{n-1}, \mathbf{u}_e^n \\ &= \frac{1}{3}(2\mathbf{U}_M^n + \mathbf{U}_E^n) + \mathbf{Z}_e^{n-1}, \end{aligned}$$

and similarly for $\mathbf{u}_e^n, \mathbf{u}_w^n, \mathbf{u}_s^n, \mathbf{u}_n^n, \mathbf{u}_{ne}^n, \mathbf{u}_{nw}^n, \mathbf{u}_{se}^n, \mathbf{u}_{sw}^n$. But the solution recomposed with the correct \mathbf{Z}^n would be:

$$\begin{aligned} \mathbf{u}_m^n &= 5\mathbf{U}_M^n - \mathbf{U}_E^n - \mathbf{U}_W^n - \mathbf{U}_S^n - \mathbf{U}_N^n - \mathbf{Z}_e^{n-1} - \mathbf{Z}_w^{n-1} - \mathbf{Z}_s^{n-1} - \mathbf{Z}_n^{n-1} - \mathbf{Z}_{ne}^{n-1} \\ &\quad - \mathbf{Z}_{nw}^{n-1} - \mathbf{Z}_{se}^{n-1} - \mathbf{Z}_{sw}^{n-1} - 8\eta, \end{aligned}$$

and

$$\mathbf{u}_e^n = \frac{1}{3}(2\mathbf{U}_M^n + \mathbf{U}_E^n) + \mathbf{Z}_e^{n-1} + \eta,$$

and similarly for the other terms. Thus we make an error of η for the solution on the cells $K_e, K_w, K_s, K_n, K_{ne}, K_{nw}, K_{se}, K_{sw}$ and an error of 8η on the cell K_m which results in the formation of these small peaks. If η is small (which is linked to the analysis made in Fig. 8) this does not spoil the solution.

Remark 8. Notice that in one space dimension the size of the peaks would be smaller; freezing the \mathbf{Z} introduces an error of order η on the adjacent fine cells K_e and K_w of a coarse cell K_M and an error of order 2η on the cell K_m .

In Fig. 13 we also compare the L^2 -errors made with this multilevel computation at 37% and with a multilevel computation at 45% to the one made with a one-level computation on the coarse and fine meshes. Fig. 13 shows that the multilevel methods at 37% and 45% remain very accurate since the corresponding errors are below the errors made on the coarse grid. The method is also very stable and computations can be pursued for a long time. The oscillations observed in the errors are due to the strongly oscillating nature of the solution (the time period is 0.5) and are independent of the multilevel method. We represent in Fig. 14 a zoom of the comparison of the errors on four periods between $t = 10$ and $t = 12$.

In Fig. 15 is displayed the scheme of the cycles followed when computing with the multilevel method at 25% (which consists in repeating cycles of the form 11111222211111 after a few iterations on the fine grid), 37% (cycles of the form 1111122222211111) and 45% (cycles of the form 111112222222211111).

Moreover we liken the CPU time needed with a one-level computation made on the fine grid and with the multilevel methods at 37%, at 25% and at 45% in Table 1. We also indicate in the second column the gain of CPU time in percentage which is made when using the multilevel methods as compared to the computation on the fine grid, and in the last two columns the percentage of CPU time spent for the iterations on the fine grid and on the coarse grid. Note that the mean CPU time spent for an iteration on the fine grid is of 0.5 s and of 0.3 s for an iteration on the coarse grid.

The more time we spend on the coarse grid, the faster the computation will be. However if during one cycle we perform too many iterations on the coarse grid, the method loses its accuracy and it can become less accurate than the one-level computation on the coarse grid. Indeed we observe in Fig. 16 that with cycles of the form 1111222222221111, the variations $\frac{\mathbf{Z}^{n+1} - \mathbf{Z}^n}{\Delta t}$ for ϕ, u and v becomes very high compared to the time step (runs over 1 for u and v), and the Fig. 17 shows us that the errors become even larger than the errors made on the coarse grid.

An improvement of the multilevel method could be made by using a criterion controlling whether the way down on a coarser level is admissible and how many iterations can be made on this coarse level without spoiling the solution. A characteristic quantity could be evaluated during the multilevel computation and when it becomes too close from a critical value, a way up on a fine level would be performed.

2.5. Concluding remarks

In Part I of this article we have implemented and studied a multilevel method to approximate the solution of a hyperbolic system of conservation laws: the shallow water equations. We have introduced new incremental unknowns which enabled us to preserve the conservation property of the schemes. The numerical simulations show that the method remains accurate while enabling to decrease the time of computation although a certain number of iterations are made on the coarse grid. The method shows its best performance for simulations requiring a small space step and very fine meshes. It could be applied with improved efficiency by using an adaptative criterion which would depend on the problem to be solved (see Section 2.4). An improvement of this method could also be done by applying it locally and selectively in the spatial domain. These ideas are left to future work.

3. Part II: Analysis of some multilevel finite volume methods

As explained in the introduction the study of the stability of the multilevel finite volume methods is widely open. However we present in this part the study of two versions of the multilevel finite volume method, with increments Z of order Δx instead of Δx^2 as in Part I. The two methods are very similar. However for the first method we only conduct the stability analysis by the Von Neumann method in space dimension one for a one-dimensional transport equation (Section 3.1.1) and for the one-dimensional linear shallow water equations (Section 3.1.2); both problems are considered with space periodicity boundary condition. For the second multilevel finite volume method we conduct the stability analysis by the energy method for two-dimensional inviscid linearized shallow water equations (Section 3.2).

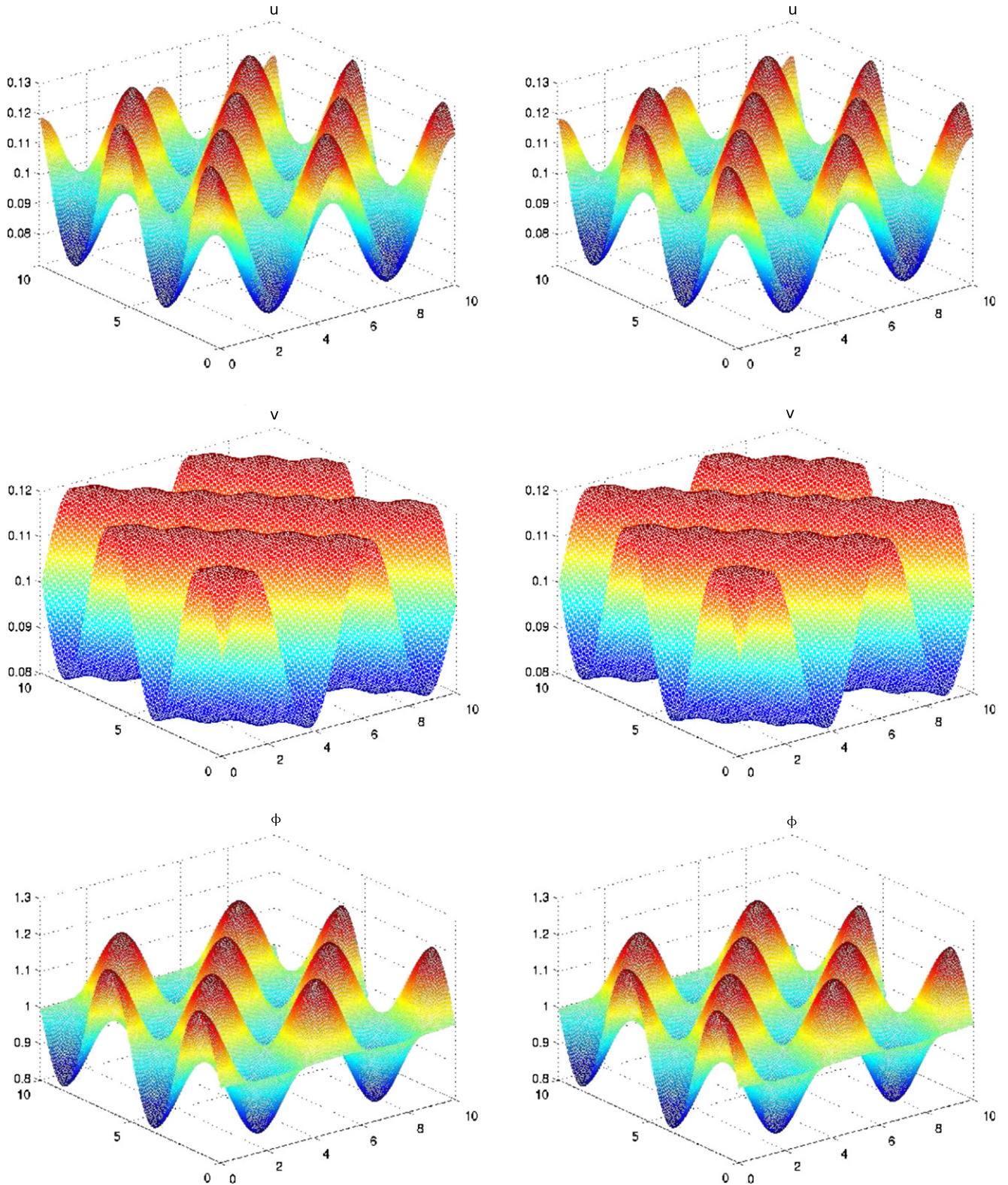


Fig. 11. Solutions obtained at $t = 20$ with a one-level computation on the fine mesh (300×300) (left), and with the multilevel method at 37% (right).

3.1. A multilevel method in space dimension one

3.1.1. The transport equation model

3.1.1.1. *Multilevel spatial discretization.* In this section we are interested in a finite volume multilevel scheme for the following linear advection equation on a one-dimensional domain $\mathcal{A} = (0, L)$:

$$\frac{\partial u}{\partial t}(x, t) + \frac{\partial u}{\partial x}(x, t) = 0. \tag{16}$$

The equation is supplemented with space periodicity boundary condition

$$u(0, t) = u(L, t), \tag{17}$$

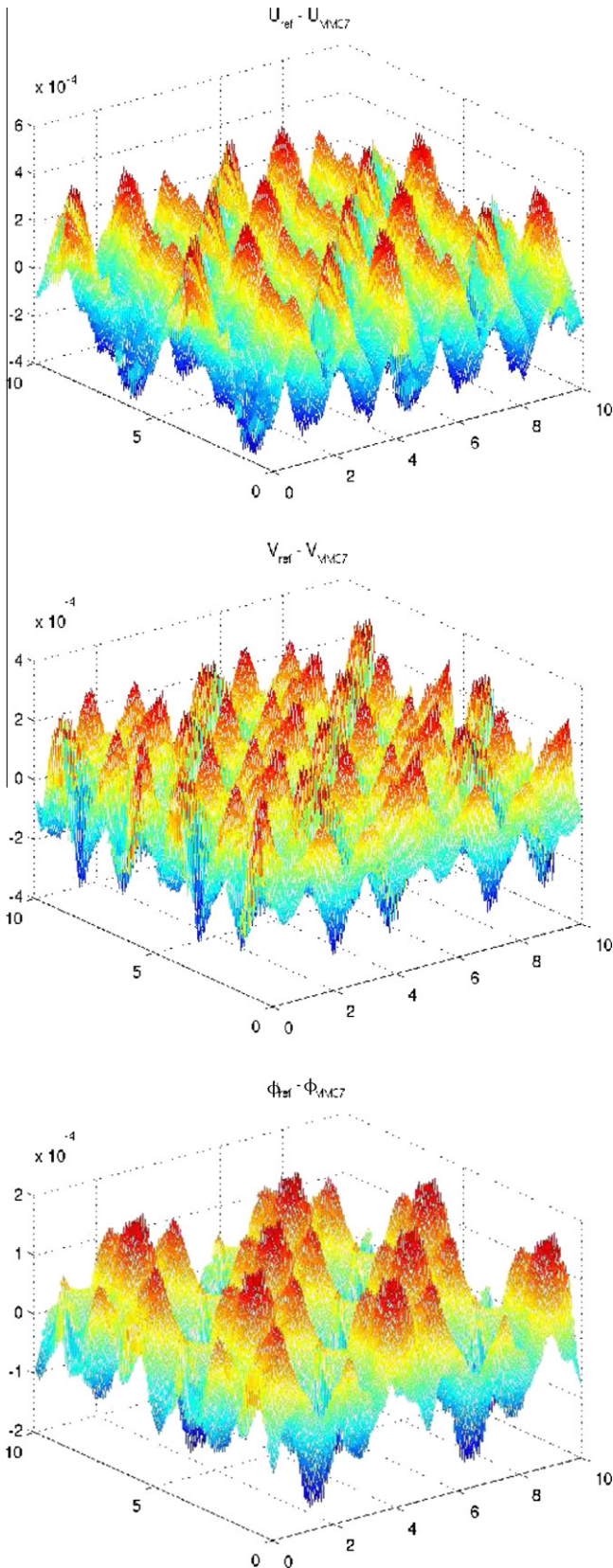


Fig. 12. Differences between the multilevel solutions ($u_{MM37}, v_{MM37}, \phi_{MM37}$) and the reference solutions ($u_{ref}, v_{ref}, \phi_{ref}$).

together with the initial condition

$$u(x, 0) = u^0(x), \tag{18}$$

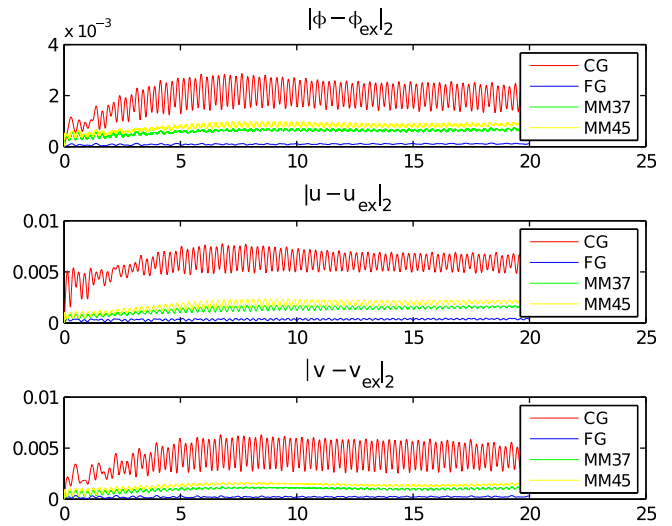


Fig. 13. Time evolution of $\|\phi - \phi_{ex}\|_2, \|u - u_{ex}\|_2, \|v - v_{ex}\|_2$ with the multilevel method at 37% (MM37) and at 45% (MM45), the computation on the fine grid (FG), and the computation on the coarse grid (CG).

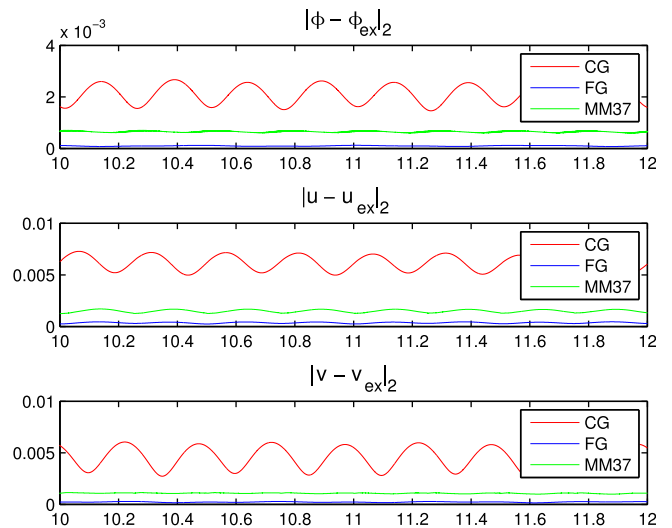


Fig. 14. Time evolution of $\|\phi - \phi_{ex}\|_2, \|u - u_{ex}\|_2, \|v - v_{ex}\|_2$ with the multilevel method at 37% (MM37), the computation on the fine grid (FG), and the computation on the coarse grid (CG).

where u^0 is some given square integrable function defined on \mathcal{M} .

The scheme will involve two grids, a fine one and a coarse one. We first introduce the fine grid consisting of $3N$ cells of uniform length Δx with $3N\Delta x = L$. Let us denote the corresponding cells by $k_j, j = 1, \dots, 3N$, so that $k_j = ((j-1)\Delta x, j\Delta x)$. The discrete unknowns on the fine grid will be denoted by $u_j, 1 \leq j \leq 3N$. Here u_j is expected to be some approximation of the mean value of u over k_j . By integrating the Eq. (16) over the cell k_j we obtain that:

$$\frac{d}{dt} \int_{(j-1)\Delta x}^{j\Delta x} u(x, t) dx + u(j\Delta x, t) - u((j-1)\Delta x, t) = 0.$$

Now the term $u(j\Delta x, t)$ is approximated by $u_j(t)$ using an ‘‘upwind’’ scheme due to the direction of the characteristics for Eq. (16). Therefore the upwind finite volume discretization reads

$$\frac{du_j}{dt}(t) + \frac{u_j(t) - u_{j-1}(t)}{\Delta x} = 0, 1 \leq j \leq 3N, \tag{19}$$

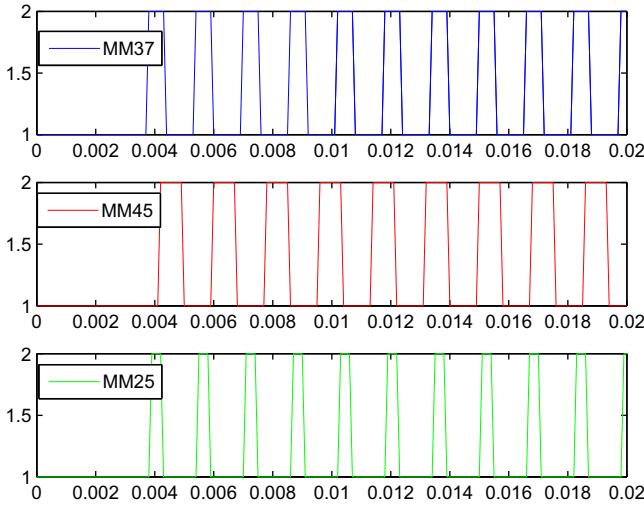


Fig. 15. Evolution of the level of discretization for different multilevel computations.

Table 1
Comparison of the CPU times used with a computation on the fine grid and with multilevel methods with different cycles. IFG = Iterations on the Fine Grid, ICG = Iterations on the Coarse Grid.

Method	CPU time	Gain in %	% IFG	% ICG
FG	26 h	–	90	0
MM25	24 h 37	5	75	13.5
MM37	22 h 21	14	66	21
MM45	21 h 55	15.6	61	26

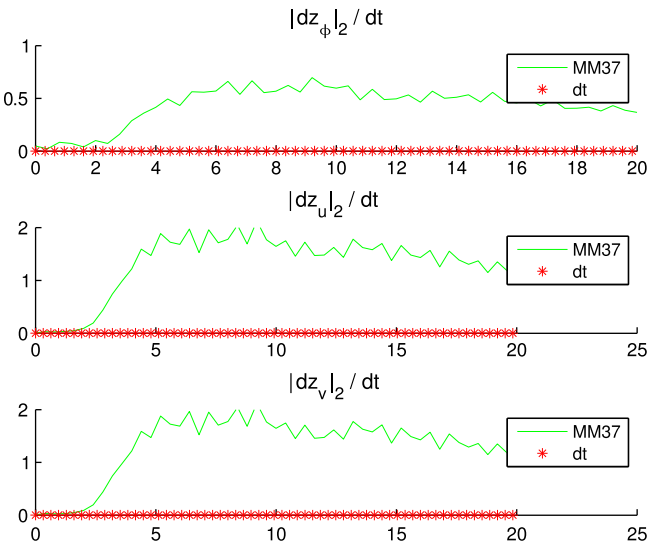


Fig. 16. Time evolution of the discrete L^2 -norms of $\frac{z^{n+1}-z^n}{\Delta t}$ for the conservative variables with the multilevel method at 50%.

where we have set

$$u_0(t) = u_{3N}(t). \tag{20}$$

These equations are supplemented with the initial conditions

$$u_j(0) = \frac{1}{\Delta x} \int_{k_j} u^0(x) dx, 1 \leq j \leq 3N. \tag{21}$$

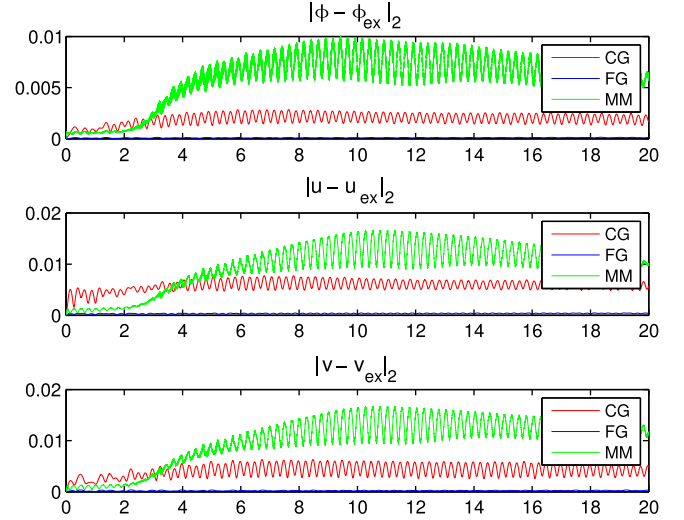


Fig. 17. Time evolution of $\|\phi - \phi_{ex}\|_2, \|u - u_{ex}\|_2, \|v - v_{ex}\|_2$ with the multilevel method at 50% (MM50), the computation on the fine grid (FG), and the computation on the coarse grid (CG).

We set $h = \Delta x$ and denote by u_h the step function which is constant on the intervals $k_j, j = 0, \dots, 3N$ with $u_h|_{k_j} = u_j$ and $u_0 = u_{3N}$. Here to take into account the boundary condition we have added the fictitious cell $k_0 = (-\Delta x, 0)$. Denoting by $\|\cdot\|_2$ the L^2 norm, we see that:

$$\|u_h\|_2^2 = \int_0^M u_h(x)^2 dx = \Delta x \sum_{j=1}^{3N} |u_j|^2. \tag{22}$$

We now introduce a coarser mesh consisting of the intervals $K_l, 1 \leq l \leq N$, with length $3\Delta x$, obtained as follows

$$K_l = k_{3l-2} \cup k_{3l-1} \cup k_{3l} = (3(l-1)\Delta x, 3l\Delta x). \tag{23}$$

Let ${}^2(u_j)_{1 \leq j \leq 3N}$ still denote the approximation of u on the fine mesh $(k_j)_{1 \leq j \leq 3N}$. Then an approximation of u on the coarse mesh is given by

$$U_l = \frac{1}{3} [u_{3l-2} + u_{3l-1} + u_{3l}], 1 \leq l \leq N, \tag{24}$$

and we introduce the incremental unknowns

$$Z_{3l-\alpha} = u_{3l-\alpha} - U_l, \tag{25}$$

where $\alpha = 0, 1, 2$ and $l = 1, \dots, N$.

Remark 9. The definition of the Z in (25) is at our disposal; in this case the Z are of order Δx . For example, using Taylor's formula we obtain

$$\begin{aligned} Z_{3l-2} &= u_{3l-2} - \frac{1}{3} [u_{3l-2} + u_{3l-1} + u_{3l}] \\ &= \frac{1}{3} [2u_{3l-2} - (u_{3l-2} + \mathcal{O}(\Delta x)) - (u_{3l-2} + \mathcal{O}(\Delta x))] = \mathcal{O}(\Delta x). \end{aligned}$$

This is to be compared with the increments of order Δx^2 considered in Part I.

The unknowns on the fine grid are thus written as the sum of the coarse grid unknowns $(U_l)_{1 \leq l \leq N}$ and the associated increments $(Z_j)_{1 \leq j \leq 3N}$.

By adding (averaging) the Eq. (19) corresponding to $j = 3l, 3l - 1$ and $3l - 2$, we obtain the following equation for U_l :

² Including, strictly speaking, the separation points.

$$\frac{dU_\ell(t)}{dt} + \frac{1}{3\Delta x}(u_{3l}(t) - u_{3l-3}(t)) = 0, 1 \leq \ell \leq N, \tag{26}$$

that also reads

$$\frac{dU_\ell(t)}{dt} + \frac{1}{3\Delta x}(U_\ell(t) - U_{\ell-1}(t)) + \frac{1}{3\Delta x}(Z_{3l}(t) - Z_{3l-3}(t)) = 0, 1 \leq \ell \leq N. \tag{27}$$

We now aim to describe the time discretization. It will rely on two different time steps Δt and $\Delta t/p$. We will perform p steps with the small time step $\Delta t/p$ and the fine space mesh $\Delta x = L/(3N)$, and then as explained below, we make q steps with the “large” time step Δt and the coarse mesh step $3\Delta x$; and then we start again with the p steps. Here $p > 1$ and $q > 1$ are two fixed integers.

3.1.1.2. The fine grid scheme with small time step. We introduce the discrete unknowns $u_j^{n+s/p}, j = 1, \dots, 3N$ that are meant to be approximations of $\frac{1}{\Delta x} \int_{k_j} u(x, t_{n+s/p}) dx$ at time $t_{n+s/p} = (n + s/p)\Delta t$. Here the $u_j^n, j = 1, \dots, 3N$, are supposed to be known and the numerical scheme will allow to determine $u_j^{n+s/p}$, for $s \geq 1$.

Coming back to Eq. (19) that we discretize in time thanks to the implicit Euler scheme, we obtain the following scheme:

$$\begin{cases} \frac{p}{\Delta t} (u_j^{n+s/p} - u_j^{n+(s-1)/p}) + \frac{1}{\Delta x} (u_j^{n+s/p} - u_{j-1}^{n+s/p}) = 0, & j = 1, \dots, 3N, \\ u_0^{n+s/p} = u_{3N}^{n+s/p}. \end{cases} \tag{28}$$

Here, since we perform p iterations of the scheme, s varies between 1 and p . We denote by $u_h^{n+s/p}$ the step functions defined for $0 \leq s \leq p$ by:

$$u_h^{n+s/p}(x) = u_j^{n+s/p}, x \in k_j, 1 \leq j \leq 3N.$$

Also, for the sake of simplicity, we will write $\tau = n + s/p, u_h^\tau = u_h^{n+s/p}$ and rewrite the scheme in the form

$$\frac{p}{\Delta t} (u_j^\tau - u_j^{\tau-1/p}) + \frac{1}{\Delta x} (u_j^\tau - u_{j-1}^\tau) = 0, j = 1, \dots, 3N. \tag{29}$$

We aim to investigate the stability of this scheme in the L^2 norm. Indeed, keeping in mind that our purpose is to investigate systems such as the shallow water equations, the L^∞ norm is not appropriate.

Since we are dealing with periodic boundary conditions, an efficient tool to express the L^2 norms is to introduce the discrete Fourier coefficients. Recall that the discrete Fourier coefficients for periodic sequences $v_j, j \in \mathbb{Z}, v_{j+3N} = v_j, h^* = \frac{2\pi}{3N}$, are defined as follows:

$$\hat{v}_m = \frac{1}{3N} \sum_{j=1}^{3N} e^{-imjh^*} v_j, m = 1, \dots, 3N. \tag{30}$$

We then have the discrete Parseval formula

$$\sum_{m=1}^{3N} |\hat{v}_m|^2 = \frac{1}{3N} \sum_{j=1}^{3N} |v_j|^2, \tag{31}$$

see the details in e.g. [6,49]. Note that the sequence $\{\hat{v}_m\}$ is itself periodic with period $3N$, and if $(\sigma v)_j = v_{j-1}$, then

$$\widehat{\sigma v}_m = e^{-imh^*} \hat{v}_m. \tag{32}$$

Hence, in view of (31) and (22), the L^2 norm of the approximation u_h^τ satisfies

$$\|u_h^\tau\|_2^2 = 3N\Delta x \sum_{m=1}^{3N} |\hat{u}_m^\tau|^2. \tag{33}$$

Next, (29) is rewritten as

$$\left(1 + \frac{\Delta t}{p\Delta x}\right) u_j^\tau - \frac{\Delta t}{p\Delta x} u_{j-1}^\tau = u_j^{\tau-1/p}, \tag{34}$$

that is for the discrete Fourier coefficients defined as in (30), where $h^* = \frac{2\pi}{3N}$,

$$\left(1 + \frac{\Delta t}{p\Delta x}(1 - e^{-imh^*})\right) \hat{u}_m^\tau = \hat{u}_m^{\tau-1/p}, m = 1, \dots, 3N. \tag{35}$$

Hence, the amplification factor for the fine mesh is,

$$g_{F,m} = \left[1 + \frac{\Delta t}{p\Delta x}(1 - e^{-imh^*})\right]^{-1}, m = 1, \dots, 3N. \tag{36}$$

We observe that

$$g_{F,m}^{-1} = \left[1 + \frac{\Delta t}{p\Delta x}(1 - \cos(h^*m)) + i \frac{\Delta t}{p\Delta x} \sin(h^*m)\right],$$

$$\|g_{F,m}^{-1}\|_2^2 = 1 + 2(1 - \cos(h^*m)) \left(\left(\frac{\Delta t}{p\Delta x}\right)^2 + \frac{\Delta t}{p\Delta x}\right),$$

and conclude that

$$\|g_{F,m}\| \leq 1, m = 1, \dots, 3N. \tag{37}$$

Coming back to (35) and (33), it follows that

$$\|u_h^\tau\|_2^2 \leq 3N\Delta x \sum_{m=1}^{3N} |\hat{u}_m^{\tau-1/p}|^2 = \|u_h^{\tau-1/p}\|_2^2.$$

Recall that $\tau = n + s/p, s = 1, \dots, p$. A straightforward induction argument allows to conclude that, for $s = 1, \dots, p$:

$$\|u_h^{n+s/p}\|_2 \leq \|u_h^n\|_2, \tag{38}$$

and therefore the p steps of the scheme (29) on the fine grid are stable for the L^2 -norm. Also, after these steps we know the approximation u_h^{n+1} at time $t_{n+1} = (n + 1)\Delta t$ (that corresponds to $s = p$).

The next q iterations will be performed on the coarse grid as explained now.

3.1.1.3. The coarse grid scheme with “large” time step. The iterations will provide u_h^{n+s+1} , for $1 \leq s \leq q$, that are approximations at time $t_{n+s} = (n + s + 1)\Delta t$.

We use the multilevel decomposition introduced in [24,25] and look for $(u_j^{n+s+1})_{1 \leq j \leq 3N}$ as the sum of the coarse grid unknowns $(U_l^{n+s+1})_{1 \leq l \leq N}$ and associated increments $(Z_j^{n+s+1})_{1 \leq j \leq 3N}$. The multi-step algorithm that we consider consists in freezing the increments Z on the fine grid during the steps $n + 2, \dots, n + q + 1$ that is we set:

$$Z_j^{n+s+1} = Z_j^{n+1}, s = 1, \dots, q, j = 1, \dots, 3N, \tag{39}$$

$$\text{and } Z_0^{n+s+1} = Z_{3N}^{n+s+1}.$$

We discretize the Eq. (27) for U_l in time thanks to the implicit Euler scheme. This yields the following scheme:

$$\begin{aligned} \frac{1}{\Delta t} (U_l^{n+s+1} - U_l^{n+s}) + \frac{1}{3\Delta x} (U_l^{n+s+1} - U_{l-1}^{n+s+1}) + \frac{1}{3\Delta x} (Z_{3l}^{n+1} \\ - Z_{3l-3}^{n+1}) \\ = 0, 1 \leq l \leq N, \end{aligned} \tag{40}$$

where we set

$$U_0^{n+s+1} = U_N^{n+s+1}. \tag{41}$$

We perform q iterations of the scheme, so that $1 \leq s \leq q$, and the algorithm is initialized by

$$U_l^{n+1} = \frac{1}{3} [u_{3l-2}^{n+1} + u_{3l-1}^{n+1} + u_{3l}^{n+1}]. \tag{42}$$

Altogether, the multilevel method provides the approximation on the fine grid at time $(n + s + 1)\Delta t$, $1 \leq s \leq q$, given by:

$$u_{3l-\alpha}^{n+s+1} = U_l^{n+s+1} + Z_{3l-\alpha}^{n+1}, \quad 1 \leq l \leq N, 0 \leq \alpha \leq 2, \quad (43)$$

but only the terms U_l^{n+s+1} on the coarse grid need to be computed. Let u_h^{n+s+1} denote the corresponding step function: $u_h^{n+s+1} = u_j^{n+s+1}$ on k_j .

Setting $\tau = n + s + 1$ for $s = 1, \dots, q$ the above algorithm rewrites

$$u_{3l-\alpha}^\tau = U_l^\tau + Z_{3l-\alpha}^{n+1}, \quad 1 \leq l \leq N, 0 \leq \alpha \leq 2,$$

where

$$\frac{1}{\Delta t}(U_l^\tau - U_l^{\tau-1}) + \frac{1}{3\Delta x}(U_l^\tau - U_{l-1}^\tau) + \frac{1}{3\Delta x}(Z_{3l}^{n+1} - Z_{3l-3}^{n+1}) = 0. \quad (44)$$

We have $U_l^\tau + Z_{3l}^{n+1} = u_{3l}^\tau$ and $U_l^\tau - U_{l-1}^{\tau-1} = u_{3l}^\tau - u_{3l-3}^{\tau-1}$ so that (44) also reads

$$\frac{1}{\Delta t}(u_{3l}^\tau - u_{3l}^{\tau-1}) + \frac{1}{3\Delta x}(u_{3l}^\tau - u_{3l-3}^{\tau-1}) = 0. \quad (45)$$

That is, as in (34)

$$\left(1 + \frac{\Delta t}{3\Delta x}\right)u_{3l}^\tau - \frac{\Delta t}{3\Delta x}u_{3l-3}^{\tau-1} = u_{3l}^{\tau-1}. \quad (46)$$

To investigate the stability of this scheme we first consider the discrete Fourier coefficients defined as in (30):

$$\begin{aligned} \hat{u}_m^\tau &= \frac{1}{3N} \sum_{j=1}^{3N} u_j^\tau e^{-ih^*jm}, \quad h^* = \frac{2\pi}{3N}, \\ &= \frac{1}{3N} \sum_{\ell=1}^N \left(u_{3\ell}^\tau e^{-ih^*3\ell m} + u_{3\ell-1}^\tau e^{-ih^*(3\ell-1)m} + u_{3\ell-2}^\tau e^{-ih^*(3\ell-2)m} \right), \end{aligned} \quad (47)$$

$$1 \leq m \leq 3N.$$

In view of (47) we now introduce the partial discrete Fourier type coefficients:

$$\hat{u}_{(3l-\alpha),m}^\tau = \frac{1}{3N} \sum_{\ell=1}^N u_{3\ell-\alpha}^\tau e^{-ih^*3\ell m}. \quad (48)$$

Here the notation $\hat{u}_{(3l-\alpha),m}^\tau$, $0 \leq \alpha \leq 2$ emphasizes that we are not dealing with the standard discrete Fourier coefficients. We observe that this sequence is periodic in m with period $3N$ and that a Parseval relation similar to (31) holds,

$$\sum_{m=1}^{3N} |\hat{u}_{(3l-\alpha),m}^\tau|^2 = \frac{1}{3N} \sum_{\ell=1}^N |u_{3\ell-\alpha}^\tau|^2, \quad \alpha = 0, 1, 2. \quad (49)$$

Concerning the L^2 norm of the step function u_h^τ , we conclude that:

$$\|u_h^\tau\|_2^2 = \sum_{\alpha=0}^2 \sum_{\ell=1}^N \Delta x |u_{3\ell-\alpha}^\tau|^2 = 3N\Delta x \sum_{\alpha=0}^2 \sum_{m=1}^{3N} |\hat{u}_{(3\ell-\alpha),m}^\tau|^2. \quad (50)$$

In view of (50), we now aim to consider the discrete coefficients $\hat{u}_{(3\ell-\alpha),m}^\tau$. For $\alpha = 0$ we can use (46). Since $\hat{u}_{(3\ell-3),m}^\tau = \hat{u}_{(3\ell),m}^\tau e^{-3ih^*m}$, this equation yields for $m = 1, \dots, 3N$

$$\left(1 + \frac{\Delta t}{3\Delta x}\right)\hat{u}_{(3\ell),m}^\tau - \frac{\Delta t}{3\Delta x}e^{-3ih^*m}\hat{u}_{(3\ell),m}^\tau = \hat{u}_{(3\ell),m}^{\tau-1}, \quad (51)$$

so that

$$\hat{u}_{(3\ell),m}^\tau = g_{C,m} \hat{u}_{(3\ell),m}^{\tau-1}, \quad g_{C,m}^{-1} = 1 + \frac{\Delta t}{3\Delta x} (1 - e^{-3ih^*m}). \quad (52)$$

Here the amplification factor $g_{C,m}$ on the coarse grid is similar to the one on the fine grid (see (36)) and, as above, we conclude that

$$|g_{C,m}| \leq 1, \quad m = 1, \dots, 3N. \quad (53)$$

Also recalling that $\tau = n + s + 1$, (52) provides

$$\hat{u}_{(3\ell),m}^{n+s+1} = g_{C,m}^s \hat{u}_{(3\ell),m}^{n+1}, \quad m = 1, \dots, 3N, \quad s = 1, \dots, q. \quad (54)$$

We now need to handle $\hat{u}_{(3\ell-1),m}$ and $\hat{u}_{(3\ell-2),m}$ but we have no equations similar to (52) for these quantities. We will look for the expressions of the $\hat{u}_{(3\ell-\alpha),m}^{n+s+1}$, $\alpha = 1, 2$, in terms of the $\hat{u}_{(3\ell-\beta),m}^{n+1}$ with $\beta = 0, 1, 2$; that of $\hat{u}_{(3\ell),m}^{n+s+1}$ has been already found and is given by (54).

The relations (43) give for the partial discrete Fourier series

$$\hat{u}_{(3\ell-\alpha),m}^{n+s+1} = \hat{U}_{(\ell),m}^{n+s+1} + \hat{Z}_{(3\ell-\alpha),m}^{n+1}, \quad (55)$$

where

$$\hat{U}_{(\ell),m}^{n+s+1} = \frac{1}{3N} \sum_{\ell=1}^N U_\ell^{n+s+1} e^{-ih^*3\ell m}$$

Using again (42) for $\alpha = 0$ and (54), we obtain the following expression of $\hat{U}_{(\ell),m}^{n+s+1}$:

$$\hat{U}_{(\ell),m}^{n+s+1} = g_{C,m}^s \hat{u}_{(3\ell),m}^{n+1} - \hat{Z}_{(3\ell),m}^{n+1}, \quad m = 1, \dots, 3N. \quad (56)$$

There remains to express $\hat{Z}_{(3\ell-\alpha),m}^{n+1}$ in terms of the $\hat{u}_{(3\ell-\beta),m}^{n+1}$, $\beta = 0, 1, 2$. Using (42), we have

$$\begin{cases} Z_{3\ell}^{n+1} = u_{3\ell}^{n+1} - U_\ell^{n+1} = \frac{1}{3}(2u_{3\ell}^{n+1} - u_{3\ell-1}^{n+1} - u_{3\ell-2}^{n+1}), \\ Z_{3\ell-1}^{n+1} = u_{3\ell-1}^{n+1} - U_\ell^{n+1} = \frac{1}{3}(2u_{3\ell-1}^{n+1} - u_{3\ell-1}^{n+1} - u_{3\ell-2}^{n+1}), \\ Z_{3\ell-2}^{n+1} = u_{3\ell-2}^{n+1} - U_\ell^{n+1} = \frac{1}{3}(2u_{3\ell-2}^{n+1} - u_{3\ell-1}^{n+1} - u_{3\ell-2}^{n+1}). \end{cases} \quad (57)$$

Thus for the partial Fourier coefficients, for $m = 1, \dots, 3N$,

$$\begin{cases} \hat{Z}_{(3\ell),m}^{n+1} = \frac{1}{3}(2\hat{u}_{(3\ell),m}^{n+1} - \hat{u}_{(3\ell-1),m}^{n+1} - \hat{u}_{(3\ell-2),m}^{n+1}), \\ \hat{Z}_{(3\ell-1),m}^{n+1} = \frac{1}{3}(2\hat{u}_{(3\ell-1),m}^{n+1} - \hat{u}_{(3\ell),m}^{n+1} - \hat{u}_{(3\ell-2),m}^{n+1}), \\ \hat{Z}_{(3\ell-2),m}^{n+1} = \frac{1}{3}(2\hat{u}_{(3\ell-2),m}^{n+1} - \hat{u}_{(3\ell),m}^{n+1} - \hat{u}_{(3\ell-1),m}^{n+1}). \end{cases} \quad (58)$$

Combining (55), (56) and (58), we conclude that:

$$\hat{u}_{(3\ell-1),m}^{n+s+1} = (g_{C,m}^s - 1)\hat{u}_{(3\ell),m}^{n+1} + \hat{u}_{(3\ell-1),m}^{n+1}, \quad (59)$$

$$\hat{u}_{(3\ell-2),m}^{n+s+1} = (g_{C,m}^s - 1)\hat{u}_{(3\ell),m}^{n+1} + \hat{u}_{(3\ell-2),m}^{n+1}. \quad (60)$$

Finally we rewrite (54), (59) and (60) in matricial form:

$$\begin{pmatrix} \hat{u}_{(3\ell),m}^{n+s+1} \\ \hat{u}_{(3\ell-1),m}^{n+s+1} \\ \hat{u}_{(3\ell-2),m}^{n+s+1} \end{pmatrix} = G_{C,m,s} \begin{pmatrix} \hat{u}_{(3\ell),m}^{n+1} \\ \hat{u}_{(3\ell-1),m}^{n+1} \\ \hat{u}_{(3\ell-2),m}^{n+1} \end{pmatrix}, \quad m = 1, \dots, 3N, \quad (61)$$

$$G_{C,m,s} = \begin{pmatrix} g_{C,m}^s & 0 & 0 \\ g_{C,m}^s - 1 & 1 & 0 \\ g_{C,m}^s - 1 & 0 & 1 \end{pmatrix}.$$

This gives the passing from time step $n + 1$ to time step to $n + s + 1$ for the Fourier coefficients. Now recalling that:

$$\|u_h^{n+s+1}\|_2^2 = 3N\Delta x \sum_{\alpha=0}^2 \sum_{m=1}^{3N} |\hat{u}_{(3\ell-\alpha),m}^{n+s+1}|^2$$

the stability of the scheme for passing from u^{n+1} to u^{n+s+1} is equivalent to showing that the spectral radius of $G_{C,m,s}$ is less or equal than 1, for $m = 1, \dots, 3N$. Since the eigenvalues of $G_{C,m,s}$ are 1 and $g_{C,m}^s$ and we have seen that $|g_{C,m}| \leq 1$, this property holds true and we conclude that for $s = 1, \dots, q$

$$\|u_h^{n+s+1}\|_2^2 \leq 3N\Delta x \sum_{\alpha=0}^2 \sum_{m=1}^{3N} |\hat{u}_{(3\ell-\alpha),m}^{n+1}|^2 = \|u_h^{n+1}\|_2^2. \quad (62)$$

Hence the q iterations of the scheme (40) on the fine grid are stable.

As already described, our algorithm consists in alternating p steps on the fine grid and q steps on the coarse one. Hence the n for which we perform the algorithm (28) on the fine grid with the small time step is a multiple of $q + 1$.

Therefore, combining (38) (for n multiple of $q + 1$) and (62), we conclude that the multilevel method is stable.

Theorem 1. *The multilevel scheme defined by the Eqs. (28) and (40) is stable in the L^2 norm. More precisely, for all n and $r \geq 0$*

$$\begin{aligned} \|u_h^n\|_2 &\leq \|u^0\|_2, \\ \|u_h^{r(q+1)+s/p}\|_2 &\leq \|u^0\|_2, \quad \text{for } s = 1, \dots, p. \end{aligned} \tag{63}$$

3.1.2. The linearized 1D shallow water equations

We now want to extend the previous results to the more complex case of the linearized shallow water equations in space dimension one. We are given some background constant flow $(\tilde{u}_0, \tilde{\phi}_0)$ assumed to be supersonic (supercritical):

$$\tilde{\phi}_0 > 0, \quad \tilde{u}_0 > \sqrt{g\tilde{\phi}_0}, \tag{64}$$

and the shallow water equations restricted to dimension 1 are linearized around this flow. We consider the nonconservative form of the shallow water equations as in Eq. (120) below; hence:

$$\begin{cases} \frac{\partial u}{\partial t} + \tilde{u}_0 \frac{\partial u}{\partial x} + g \frac{\partial \phi}{\partial x} = 0, \\ \frac{\partial \phi}{\partial t} + \tilde{u}_0 \frac{\partial \phi}{\partial x} + \tilde{\phi}_0 \frac{\partial u}{\partial x} = 0. \end{cases} \tag{65}$$

This system is considered on the domain $\mathcal{M} = (0, L)$ and is supplemented with the periodicity boundary conditions

$$u(0, t) = u(L, t), \phi(0, t) = \phi(L, t), \tag{66}$$

and the initial conditions

$$u(x, 0) = u^0(x), \phi(x, 0) = \phi^0(x). \tag{67}$$

Here u^0 and ϕ^0 are two given square integrable functions defined on \mathcal{M} . The existence of a solution to the continuous problem (65)–(67) will not be discussed here and we refer the reader to Section 3.2 for a two-dimensional problem.

The multilevel discretization relies on the space meshes described in Section 3.1.1.1. As above we will perform p iterations on the fine grid (with timestep $\Delta t/p$) that will yield the two step functions

$$u_h^{n+s/p} = u_j^{n+s/p} \quad \text{and} \quad \phi_h^{n+s/p} = \phi_j^{n+s/p} \quad \text{on } k_j, \quad 1 \leq j \leq 3N, \quad 1 \leq s \leq p,$$

followed by q iterations on the coarse grid (with timestep Δt) yielding the approximations

$$u_h^{n+s+1} = u_j^{n+s+1} \quad \text{and} \quad \phi_h^{n+s+1} = \phi_j^{n+s+1} \quad \text{on } k_j, \quad 1 \leq j \leq 3N, \quad 1 \leq s \leq q.$$

3.1.2.1. Fine grid scheme with “small” time step. The fine grid scheme reads (compare to (28) and (29))

$$\begin{cases} \frac{p}{\Delta t} (u_j^\tau - u_j^{\tau-1/p}) + \frac{\tilde{u}_0}{\Delta x} (u_j^\tau - u_{j-1}^\tau) + \frac{g}{\Delta x} (\phi_j^\tau - \phi_{j-1}^\tau) = 0, \\ \frac{p}{\Delta t} (\phi_j^\tau - \phi_j^{\tau-1/p}) + \frac{\tilde{u}_0}{\Delta x} (\phi_j^\tau - \phi_{j-1}^\tau) + \frac{\tilde{\phi}_0}{\Delta x} (u_j^\tau - u_{j-1}^\tau) = 0, \end{cases} \tag{68}$$

where $\tau = n + s/p$, $s = 1, \dots, p$, $j = 1, \dots, 3N$, $u_0^\tau = u_{3N}^\tau$, $\phi_0^\tau = \phi_{3N}^\tau$ by space periodicity. The scheme also reads

$$\begin{cases} \left(1 + \frac{\tilde{u}_0}{p} \frac{\Delta t}{\Delta x}\right) u_j^\tau - \frac{\tilde{u}_0}{p} \frac{\Delta t}{\Delta x} u_{j-1}^\tau + \frac{g}{p} \frac{\Delta t}{\Delta x} (\phi_j^\tau - \phi_{j-1}^\tau) = u_j^{\tau-1/p}, \\ \left(1 + \frac{\tilde{u}_0}{p} \frac{\Delta t}{\Delta x}\right) \phi_j^\tau - \frac{\tilde{u}_0}{p} \frac{\Delta t}{\Delta x} \phi_{j-1}^\tau + \frac{\tilde{\phi}_0}{p} \frac{\Delta t}{\Delta x} (u_j^\tau - u_{j-1}^\tau) = \phi_j^{\tau-1/p}. \end{cases} \tag{69}$$

From this, we deduce for the discrete Fourier coefficients \hat{u}_m^τ and $\hat{\phi}_m^\tau$, $m = 1, \dots, 3N$ defined as in (30), that

$$\begin{cases} \left(1 + \frac{\tilde{u}_0}{p} \frac{\Delta t}{\Delta x} (1 - e^{-imh^*})\right) \hat{u}_m^\tau + \frac{g}{p} \frac{\Delta t}{\Delta x} \hat{\phi}_m^\tau (1 - e^{-imh^*}) = \hat{u}_m^{\tau-1/p}, \\ \left(1 + \frac{\tilde{u}_0}{p} \frac{\Delta t}{\Delta x} (1 - e^{-imh^*})\right) \hat{\phi}_m^\tau + \frac{\tilde{\phi}_0}{p} \frac{\Delta t}{\Delta x} \hat{u}_m^\tau (1 - e^{-imh^*}) = \hat{\phi}_m^{\tau-1/p}. \end{cases} \tag{70}$$

These two equations can be rewritten in matricial form:

$$\begin{pmatrix} \hat{u}_m^\tau \\ \hat{\phi}_m^\tau \end{pmatrix} = G_{F,m} \begin{pmatrix} \hat{u}_m^{\tau-1/p} \\ \hat{\phi}_m^{\tau-1/p} \end{pmatrix}, \tag{71}$$

where the matrix $G_{F,m}$ is of order two and given by

$$G_{F,m}^{-1} = \begin{pmatrix} 1 + \frac{\tilde{u}_0}{p} \frac{\Delta t}{\Delta x} (1 - e^{-imh^*}) & \frac{g}{p} \frac{\Delta t}{\Delta x} (1 - e^{-imh^*}) \\ \frac{\tilde{\phi}_0}{p} \frac{\Delta t}{\Delta x} (1 - e^{-imh^*}) & 1 + \frac{\tilde{u}_0}{p} \frac{\Delta t}{\Delta x} (1 - e^{-imh^*}) \end{pmatrix}.$$

Recalling (64), the eigenvalues of $G_{F,m}^{-1}$ are easily computed

$$\rho_{\pm,m} = 1 + \Lambda_\pm (1 - e^{-imh^*}) \quad \text{with} \quad \Lambda_\pm = \frac{1}{p} (\tilde{u}_0 \pm \sqrt{g\tilde{\phi}_0}) \frac{\Delta t}{\Delta x}.$$

Note that (64) then implies that $\Lambda_\pm > 0$ so that

$$|\rho_{\pm,m}|^2 = 1 + 2(1 - \cos(h^*m))(\Lambda_\pm^2 + \Lambda_\pm) \geq 1, \quad m = 1, \dots, 3N.$$

Hence, the spectral radius of $G_{F,m}$ is less or equal to one. Consequently (71) provides:

$$|\hat{u}_m^\tau|^2 + |\hat{\phi}_m^\tau|^2 \leq |\hat{u}_m^{\tau-1/p}|^2 + |\hat{\phi}_m^{\tau-1/p}|^2, \quad m = 1, \dots, 3N. \tag{72}$$

Similarly to (38), we infer from this inequality that

$$\|u_h^{n+s/p}\|_2^2 + \|\phi_h^{n+s/p}\|_2^2 \leq \|u_h^n\|_2^2 + \|\phi_h^n\|_2^2, \quad s = 1, \dots, p, \tag{73}$$

and therefore the p steps of the scheme (68) on the fine grid are stable for the L^2 -norm.

3.1.2.2. Coarse grid scheme with “large” time step. The two approximations u_h^τ and ϕ_h^τ with $\tau = n + s + 1$ will be written as the sums of coarse grid unknowns and increments as follows (compare to (43)):

$$u_{3l-\alpha}^\tau = U_l^\tau + Z_{3l-\alpha}^{u,n+1}, \quad 1 \leq l \leq N, \quad 0 \leq \alpha \leq 2, \tag{74}$$

$$\phi_{3l-\alpha}^\tau = \Phi_l^\tau + Z_{3l-\alpha}^{\phi,n+1}, \quad 1 \leq l \leq N, \quad 0 \leq \alpha \leq 2. \tag{75}$$

Then, the analog of scheme (40) and (44) reads

$$\begin{cases} \frac{1}{\Delta t} (U_l^\tau - U_l^{\tau-1}) + \frac{\tilde{u}_0}{3\Delta x} (U_l^\tau - U_{l-1}^\tau) + \frac{\tilde{u}_0}{3\Delta x} (Z_{3l}^{u,n+1} - Z_{3l-3}^{u,n+1}) \\ \quad + \frac{g}{3\Delta x} (\Phi_{3l}^\tau - \Phi_{3l-3}^\tau) + \frac{g}{3\Delta x} (Z_{3l}^{\phi,n+1} - Z_{3l-3}^{\phi,n+1}) = 0, \\ \frac{1}{\Delta t} (\Phi_l^\tau - \Phi_l^{\tau-1}) + \frac{\tilde{u}_0}{3\Delta x} (\Phi_{3l}^\tau - \Phi_{3l-3}^\tau) + \frac{\tilde{u}_0}{3\Delta x} (Z_{3l}^{\phi,n+1} - Z_{3l-3}^{\phi,n+1}) \\ \quad + \frac{\tilde{\phi}_0}{3\Delta x} (U_l^\tau - U_{l-1}^\tau) + \frac{\tilde{\phi}_0}{3\Delta x} (Z_{3l}^{u,n+1} - Z_{3l-3}^{u,n+1}) = 0, \end{cases} \tag{76}$$

for $\tau = n + s + 1$, $s = 1, \dots, q$ and $l = 1, \dots, N$. Since $U_l^\tau - U_l^{\tau-1} = u_{3l}^\tau - u_{3l}^{\tau-1}$ and $\Phi_l^\tau - \Phi_l^{\tau-1} = \phi_{3l}^\tau - \phi_{3l}^{\tau-1}$, (76) also reads:

$$\begin{cases} \frac{1}{\Delta t} (u_{3l}^\tau - u_{3l}^{\tau-1}) + \frac{\tilde{u}_0}{3\Delta x} (u_{3l}^\tau - u_{3l-3}^\tau) + \frac{g}{3\Delta x} (\phi_{3l}^\tau - \phi_{3l-3}^\tau) = 0, \\ \frac{1}{\Delta t} (\phi_{3l}^\tau - \phi_{3l}^{\tau-1}) + \frac{\tilde{u}_0}{3\Delta x} (\phi_{3l}^\tau - \phi_{3l-3}^\tau) + \frac{\tilde{\phi}_0}{3\Delta x} (u_{3l}^\tau - u_{3l-3}^\tau) = 0. \end{cases} \tag{77}$$

Hence for the partial Fourier coefficients defined as in (48), for $m = 1, \dots, 3N$:

$$\begin{pmatrix} \hat{u}_{(3l),m}^\tau \\ \hat{\phi}_{(3l),m}^\tau \end{pmatrix} = G_{C,m} \begin{pmatrix} \hat{u}_{(3l),m}^{\tau-1} \\ \hat{\phi}_{(3l),m}^{\tau-1} \end{pmatrix}, \tag{78}$$

with

$$G_{C,m}^{-1} = \begin{pmatrix} 1 + \frac{\tilde{u}_0}{3} \frac{\Delta t}{\Delta x} (1 - e^{-3ih^*m}) & \frac{g}{3} \frac{\Delta t}{\Delta x} (1 - e^{-3ih^*m}) \\ \frac{\tilde{\phi}_0}{3} \frac{\Delta t}{\Delta x} (1 - e^{-3ih^*m}) & 1 + \frac{\tilde{u}_0}{3} \frac{\Delta t}{\Delta x} (1 - e^{-3ih^*m}) \end{pmatrix}.$$

The matrix $G_{C,m}$ is very similar to $G_{F,m}$ and we prove in the same way that its spectral radius is less or equal to 1. Also, (78) provides

$$\begin{pmatrix} \hat{u}_{(3l,m)}^{n+s+1} \\ \hat{\phi}_{(3l,m)}^{n+s+1} \end{pmatrix} = G_{C,m}^s \begin{pmatrix} \hat{u}_{(3l,m)}^{n+1} \\ \hat{\phi}_{(3l,m)}^{n+1} \end{pmatrix}. \tag{79}$$

We now aim to express $\hat{u}_{(3l-\alpha,m)}^{n+s+1}, \hat{\phi}_{(3l-\alpha,m)}^{n+s+1}$ for $\alpha = 1, 2$ in terms of $\hat{u}_{(3l-\beta,m)}^{n+1}, \hat{\phi}_{(3l-\beta,m)}^{n+1}, \beta = 0, 1, 2$. Thanks to (79), we have that

$$\begin{pmatrix} \hat{U}_{(l,m)}^{n+s+1} \\ \hat{\Phi}_{(l,m)}^{n+s+1} \end{pmatrix} = \begin{pmatrix} \hat{u}_{(3l,m)}^{n+s+1} \\ \hat{\phi}_{(3l,m)}^{n+s+1} \end{pmatrix} - \begin{pmatrix} \hat{Z}_{(3l,m)}^{u,n+1} \\ \hat{Z}_{(3l,m)}^{\phi,n+1} \end{pmatrix} = G_{C,m}^s \begin{pmatrix} \hat{u}_{(3l,m)}^{n+1} \\ \hat{\phi}_{(3l,m)}^{n+1} \end{pmatrix} - \begin{pmatrix} \hat{Z}_{(3l,m)}^{u,n+1} \\ \hat{Z}_{(3l,m)}^{\phi,n+1} \end{pmatrix}. \tag{80}$$

Then, we obtain as above for (59), (60)

$$\begin{pmatrix} \hat{u}_{(3l-1,m)}^{n+s+1} \\ \hat{\phi}_{(3l-1,m)}^{n+s+1} \end{pmatrix} = (G_{C,m}^s - I_2) \begin{pmatrix} \hat{u}_{(3l,m)}^{n+1} \\ \hat{\phi}_{(3l,m)}^{n+1} \end{pmatrix} + \begin{pmatrix} \hat{u}_{(3l-1,m)}^{n+1} \\ \hat{\phi}_{(3l-1,m)}^{n+1} \end{pmatrix}, \tag{81}$$

$$\begin{pmatrix} \hat{u}_{(3l-2,m)}^{n+s+1} \\ \hat{\phi}_{(3l-2,m)}^{n+s+1} \end{pmatrix} = (G_{C,m}^s - I_2) \begin{pmatrix} \hat{u}_{(3l,m)}^{n+1} \\ \hat{\phi}_{(3l,m)}^{n+1} \end{pmatrix} + \begin{pmatrix} \hat{u}_{(3l-2,m)}^{n+1} \\ \hat{\phi}_{(3l-2,m)}^{n+1} \end{pmatrix}. \tag{82}$$

Combining (79), (81) and (82), we conclude that

$$\begin{pmatrix} \hat{u}_{(3l,m)}^{n+s+1} \\ \hat{\phi}_{(3l,m)}^{n+s+1} \\ \hat{u}_{(3l-1,m)}^{n+s+1} \\ \hat{\phi}_{(3l-1,m)}^{n+s+1} \\ \hat{u}_{(3l-2,m)}^{n+s+1} \\ \hat{\phi}_{(3l-2,m)}^{n+s+1} \end{pmatrix} = \mathcal{G}_{C,m,s} \begin{pmatrix} \hat{u}_{(3l,m)}^{n+1} \\ \hat{\phi}_{(3l,m)}^{n+1} \\ \hat{u}_{(3l-1,m)}^{n+1} \\ \hat{\phi}_{(3l-1,m)}^{n+1} \\ \hat{u}_{(3l-2,m)}^{n+1} \\ \hat{\phi}_{(3l-2,m)}^{n+1} \end{pmatrix}, m = 1, \dots, 3N, \tag{83}$$

where $\mathcal{G}_{C,m,s}$ is a matrix of order 6 given by:

$$\mathcal{G}_{C,m,s} = \begin{pmatrix} G_{C,m}^s & 0 & 0 \\ G_{C,m}^s - I_2 & I_2 & 0 \\ G_{C,m}^s - I_2 & 0 & I_2 \end{pmatrix}.$$

All the eigenvalues of $\mathcal{G}_{C,m,s}$ are less than or equal to 1 in magnitude (since the same holds true for $G_{C,m}$). Therefore, we conclude as for (62) that:

$$\|u_h^{n+s+1}\|_2^2 + \|\phi_h^{n+s+1}\|_2^2 \leq \|u_h^{n+1}\|_2^2 + \|\phi_h^{n+1}\|_2^2, \text{ for } s = 1, \dots, q,$$

which yields the stability of the scheme (76) going from time step $(n + 1)\Delta t$ to time step $(n + s + 1)\Delta t$.

Theorem 2. *The multilevel scheme defined by Eqs. (68) and (76) is stable in the L^2 -norm. More precisely, for all n and $r \geq 0$:*

$$\begin{aligned} \|u_h^n\|_2^2 + \|\phi_h^n\|_2^2 &\leq \|u_h^0\|_2^2 + \|\phi_h^0\|_2^2, \\ \|u_h^{r(q+1)+s/p}\|_2^2 + \|\phi_h^{r(q+1)+s/p}\|_2^2 &\leq \|u_h^0\|_2^2 + \|\phi_h^0\|_2^2, \text{ for } s = 1, \dots, p. \end{aligned} \tag{85}$$

3.2. A multilevel method in space dimension two

We now present a different multilevel method for the two dimensional Shallow Water equations linearized around a constant flow $(\tilde{u}_0, \tilde{v}_0, \tilde{\phi}_0)$ (see Eq. (87) below). As in the previous section we linearize the 2D shallow water equations considered in their non-conservative form corresponding to (120) below. Another difference with Section 3.1.2 is that the boundary conditions are not periodic anymore. As shown in [32], the boundary conditions which can be associated with these equations depend on the relative values of the velocities ($\tilde{u}_0^2, \tilde{v}_0^2 >$ or $< g\tilde{\phi}_0$), that is whether

these velocities are sub- or supercritical (sub- or supersonic). We consider here the case where

$$\tilde{\phi}_0 > 0, \quad \tilde{u}_0 > \sqrt{g\tilde{\phi}_0}, \quad \tilde{v}_0 > \sqrt{g\tilde{\phi}_0}, \tag{86}$$

for which the boundary conditions ought to be specified at $x = 0$ and $y = 0$; we will consider homogeneous boundary conditions.

3.2.1. The equations

We consider in the domain $\mathcal{M} = (0, L_x) \times (0, L_y)$ the equations

$$\begin{cases} \frac{\partial u}{\partial t} + \tilde{u}_0 \frac{\partial u}{\partial x} + \tilde{v}_0 \frac{\partial u}{\partial y} + g \frac{\partial \phi}{\partial x} = 0, \\ \frac{\partial v}{\partial t} + \tilde{u}_0 \frac{\partial v}{\partial x} + \tilde{v}_0 \frac{\partial v}{\partial y} + g \frac{\partial \phi}{\partial y} = 0, \\ \frac{\partial \phi}{\partial t} + \tilde{u}_0 \frac{\partial \phi}{\partial x} + \tilde{v}_0 \frac{\partial \phi}{\partial y} + \tilde{\phi}_0 \left(\frac{\partial u}{\partial x} + \frac{\partial v}{\partial y} \right) = 0. \end{cases} \tag{87}$$

For the subcritical flow under consideration, we supplement (87) with the boundary conditions:

$$\mathbf{u} = (u, v, \phi) = 0, \quad \text{at } \{x = 0\} \cup \{y = 0\}, \tag{88}$$

and the initial conditions

$$\begin{aligned} u(x, y, 0) &= u^0(x, y), \quad v(x, y, 0) = v^0(x, y), \\ &\quad \times \phi(x, y, 0) = \phi^0(x, y). \end{aligned}$$

Here u^0, v^0 and ϕ^0 are three given square integrable functions defined on \mathcal{M} .

The existence of a solution to the continuous problem (87)–(89) relies on energy estimates. Since we will somehow mimic these estimates when proving the stability of the multilevel scheme below, we start by deriving them.

Theorem 3. *Under the assumption (86), for all sufficiently smooth (u, v, ϕ) solution of (87)–(89), the quantity*

$$\begin{aligned} &\int \int_{\mathcal{M}} u(x, y, t)^2 dx dy + \int \int_{\mathcal{M}} v(x, y, t)^2 dx dy \\ &+ \frac{g}{\tilde{\phi}_0} \int \int_{\mathcal{M}} \phi(x, y, t)^2 dx dy \end{aligned}$$

is a decreasing function of time t . In particular, its value at time $t > 0$ is bounded by its value at $t = 0$ corresponding to the initial conditions.

Proof. Hereafter we set $\mathbf{u} = (u, v, \phi)$ and denote

$$\begin{aligned} \|\mathbf{u}(t)\|_2^2 &= \int \int_{\mathcal{M}} u(x, y, t)^2 dx dy + \int \int_{\mathcal{M}} v(x, y, t)^2 dx dy \\ &+ \frac{g}{\tilde{\phi}_0} \int \int_{\mathcal{M}} \phi(x, y, t)^2 dx dy. \end{aligned}$$

To estimate $\|\mathbf{u}(t)\|_2^2$, we use the Eq. (87): we multiply the equation for u by u , the one for v by v , the one for ϕ by $\frac{g}{\tilde{\phi}_0} \phi$ and integrate over \mathcal{M} . Adding the corresponding equalities, we obtain the following identity

$$\frac{1}{2} \frac{d}{dt} \|\mathbf{u}(t)\|_2^2 + I^1(t) + I^2(t) = 0, \tag{90}$$

with

$$I^1(t) = \int \int_{\mathcal{M}} \left[\tilde{u}_0 u_x u + g \phi_x u + \tilde{u}_0 v_x v + \frac{g}{\tilde{\phi}_0} \tilde{u}_0 \phi_x \phi + g u_x \phi \right] dx dy,$$

$$I^2(t) = \int \int_{\mathcal{M}} \left[\tilde{v}_0 v_y v + g \phi_y v + \tilde{v}_0 u_y u + \frac{g}{\tilde{\phi}_0} \tilde{v}_0 \phi_y \phi + g v_y \phi \right] dx dy.$$

Then

$$\begin{aligned}
I^1(t) &= \frac{\tilde{u}_0}{2} \int \int_{\mathcal{M}} \left[(u^2)_x + (v^2)_x + \frac{g}{\phi_0} (\phi^2)_x \right] dx dy \\
&\quad + \int \int_{\mathcal{M}} g(\phi u)_x dx dy, \\
&= \frac{\tilde{u}_0}{2} \int_0^{L_y} \left[u^2 + v^2 + \frac{g}{\phi_0} \phi^2 \right]_{x=0}^{x=L_x} dy + \int_0^{L_y} [g(\phi u)]_{x=0}^{x=L_x} dy. \quad (91)
\end{aligned}$$

Recall that $\mathbf{u} = \mathbf{0}$ at $x = 0$. Also the assumption (86) yields that

$$\frac{\tilde{u}_0}{2} u^2 + \frac{\tilde{u}_0}{2} \frac{g}{\phi_0} \phi^2 + g\phi u$$

is pointwise positive. Therefore we infer from (91) that $I^1(t) \geq 0$. A similar computation provides $I^2(t) \geq 0$. Coming back to (90), we conclude that $\frac{d}{dt} \|\mathbf{u}(t)\|_2^2 \leq 0$. \square

In view of Theorem 3, we will equip $L^2(\mathcal{M})^3$ with the following norm (which is not the standard L^2 norm): for $(u_1, u_2, u_3) \in L^2(\mathcal{M})^3$, we set

$$\begin{aligned}
\|(u_1, u_2, u_3)\|_2^2 &= \int \int_{\mathcal{M}} u_1(x, y)^2 dx dy + \int \int_{\mathcal{M}} u_2(x, y)^2 dx dy \\
&\quad + \frac{g}{\phi_0} \int \int_{\mathcal{M}} u_3(x, y)^2 dx dy. \quad (92)
\end{aligned}$$

The fact that the boundary and initial value problem (87), (88), (89) is well posed is a recent result proved in [33].

3.2.2. Multilevel finite volumes spatial discretization

We decompose $\mathcal{M} = (0, L_x) \times (0, L_y)$ into $3N_x \times 3N_y$ rectangles of size $\Delta x \times \Delta y$ with $3N_x \Delta x = L_x$ and $3N_y \Delta y = L_y$; the rectangles are denoted by k_{ij} :

$$k_{ij} = ((i-1)\Delta x, i\Delta x) \times ((j-1)\Delta y, j\Delta y), \quad 1 \leq i \leq 3N_x, \quad 1 \leq j \leq 3N_y.$$

For the boundary conditions we add fictitious cells on the West and South sides:

$$k_{0j} = (-\Delta x, 0) \times ((j-1)\Delta y, j\Delta y), \quad 1 \leq j \leq 3N_y,$$

and

$$k_{i0} = ((i-1)\Delta x, i\Delta x) \times (-\Delta y, 0), \quad 1 \leq i \leq 3N_x.$$

As in the 1D case, the finite volume scheme is found by integrating the Eq. (87) over each control volume k_{ij} . We approximate the unknowns $\mathbf{u} = (u, v, \phi)$ with the step functions $\mathbf{u}_h(x, y, t) = \mathbf{u}_{ij}(t)$ for $(x, y) \in k_{ij}$ and since $\tilde{u}_0 > 0$ and $\tilde{v}_0 > 0$ we use an upwind scheme for the fluxes. This yields the following semi-discrete equations for $\mathbf{u}_{ij}(t) = (u_{ij}(t), v_{ij}(t), \phi_{ij}(t))$:

$$\begin{cases}
\frac{d}{dt} u_{ij} + \tilde{u}_0 \frac{u_{ij} - u_{i-1,j}}{\Delta x} + \tilde{v}_0 \frac{u_{ij} - u_{i,j-1}}{\Delta y} + g \frac{\phi_{ij} - \phi_{i-1,j}}{\Delta x} = 0, \\
\frac{d}{dt} v_{ij} + \tilde{u}_0 \frac{v_{ij} - v_{i-1,j}}{\Delta x} + \tilde{v}_0 \frac{v_{ij} - v_{i,j-1}}{\Delta y} + g \frac{\phi_{ij} - \phi_{i,j-1}}{\Delta y} = 0, \\
\frac{d}{dt} \phi_{ij} + \tilde{u}_0 \frac{\phi_{ij} - \phi_{i-1,j}}{\Delta x} + \tilde{v}_0 \frac{\phi_{ij} - \phi_{i,j-1}}{\Delta y} + \tilde{\phi}_0 \left(\frac{u_{ij} - u_{i-1,j}}{\Delta x} + \frac{v_{ij} - v_{i,j-1}}{\Delta y} \right) = 0, \\
\mathbf{u}_{0j} = \mathbf{u}_{i,0} = 0, \\
\mathbf{u}_{ij}(0) = \mathbf{u}_{ij}^0,
\end{cases} \quad (93)$$

where

$$\mathbf{u}^0 = (u^0, v^0, \phi^0), \quad \mathbf{u}_{ij}^0 = \frac{1}{\Delta x \Delta y} \int_{k_{ij}} \mathbf{u}^0(x, y) dx dy. \quad (94)$$

Introducing the finite difference operators:

$$\delta_h^x g_h = \frac{1}{\Delta x} (g_{ij} - g_{i-1,j}), \quad \delta_h^y g_h = \frac{1}{\Delta y} (g_{ij} - g_{i,j-1}) \quad \text{on } k_{ij},$$

the semi-discretized equations also read

$$\begin{cases}
\frac{d}{dt} u_h + \tilde{u}_0 \delta_h^x u_h + \tilde{v}_0 \delta_h^y u_h + g \delta_h^x \phi_h = 0, \\
\frac{d}{dt} v_h + \tilde{u}_0 \delta_h^x v_h + \tilde{v}_0 \delta_h^y v_h + g \delta_h^y \phi_h = 0, \\
\frac{d}{dt} \phi_h + \tilde{u}_0 \delta_h^x \phi_h + \tilde{v}_0 \delta_h^y \phi_h + \tilde{\phi}_0 (\delta_h^x u_h + \delta_h^y v_h) = 0,
\end{cases} \quad (95)$$

where $(u_h, v_h, \phi_h) = (u_{ij}, v_{ij}, \phi_{ij})$ on k_{ij} .

We next introduce the coarse mesh consisting³ of the rectangles $K_{lm}, 1 \leq l \leq N_x, 1 \leq m \leq N_y$:

$$K_{lm} = \bigcup_{\alpha, \beta=0}^2 k_{3l-\alpha, 3m-\beta} = (3(l-1)\Delta x, 3l\Delta x) \times (3(m-1)\Delta y, 3m\Delta y).$$

We also define the fictitious rectangles $K_{0,m}, K_{l,0}, l = 1, \dots, N_x, m = 1, \dots, N_y$, needed for the implementation of the boundary conditions; they are defined as above with m or $l = 0$.

If $\mathbf{u}_h = \mathbf{u}_{ij}$ on k_{ij} still denotes the approximation of \mathbf{u} on the fine mesh, we introduce for $l = 1, \dots, N_x$ and $m = 1, \dots, N_y$ the averages

$$\mathbf{U}_{l,m} = \frac{1}{9} \sum_{\alpha, \beta=0}^2 \mathbf{u}_{3l-\alpha, 3m-\beta} \quad (96)$$

and the incremental unknowns

$$\mathbf{Z}_{3l-\alpha, 3m-\beta} = \mathbf{u}_{3l-\alpha, 3m-\beta} - \mathbf{U}_{l,m}, \quad \alpha = 0, 1, 2, \quad (97)$$

which satisfy the following algebraic relations for $l = 1, \dots, N_x$ and $m = 1, \dots, N_y$:

$$\sum_{\alpha, \beta=0}^2 \mathbf{Z}_{3l-\alpha, 3m-\beta} = \mathbf{0}. \quad (98)$$

Let us denote by $(U_{l,m}, V_{l,m}, \Phi_{l,m})$ the components of $\mathbf{U}_{l,m}$ and by $(Z_{ij}^u, Z_{ij}^v, Z_{ij}^\phi)$ the ones of \mathbf{Z}_{ij} . Also, let \mathbf{U}_{3h} be the step function equal to \mathbf{U}_{lm} on K_{lm} (on the coarse mesh) and let \mathbf{Z}_h be the step function equal to \mathbf{Z}_{ij} on k_{ij} (on the fine mesh).

The unknown \mathbf{u}_h on the fine grid is thus written as the sum of the coarse grid unknowns \mathbf{U}_{3h} and the associated increments \mathbf{Z}_h . With this in mind, we consider a coarse grid discretization of the equations similar to (95), that is

$$\begin{cases}
\frac{d}{dt} U_{3h} + \tilde{u}_0 \delta_{3h}^x U_{3h} + \tilde{v}_0 \delta_{3h}^y U_{3h} + g \delta_{3h}^x \Phi_{3h} = 0, \\
\frac{d}{dt} V_{3h} + \tilde{u}_0 \delta_{3h}^x V_{3h} + \tilde{v}_0 \delta_{3h}^y V_{3h} + g \delta_{3h}^y \Phi_{3h} = 0, \\
\frac{d}{dt} \Phi_{3h} + \tilde{u}_0 \delta_{3h}^x \Phi_{3h} + \tilde{v}_0 \delta_{3h}^y \Phi_{3h} + \tilde{\phi}_0 (\delta_{3h}^x U_{3h} + \delta_{3h}^y V_{3h}) = 0,
\end{cases} \quad (99)$$

with $\mathbf{U}_{3h} = \mathbf{0}$ on the fictitious cells $K_{0,m}$ and $K_{l,0}$ for $l = 1, \dots, N_x, m = 1, \dots, N_y$.

The multilevel spatial decomposition is well adapted for estimating the L^2 norms. Indeed, considering some component of \mathbf{u}_h , for example the first one u_h , we infer from (97) and (98) that:

$$\begin{aligned}
\sum_{\alpha, \beta=0}^2 |u_{3l-\alpha, 3m-\beta}|^2 &= \sum_{\alpha, \beta=0}^2 |U_{l,m} + Z_{3l-\alpha, 3m-\beta}^u|^2 \\
&= 9|U_{l,m}|^2 + \sum_{\alpha, \beta=0}^2 |Z_{3l-\alpha, 3m-\beta}^u|^2. \quad (100)
\end{aligned}$$

Multiplying (100) by $\Delta x \Delta y$ and adding the resulting equations for $l = 1, \dots, N_x, m = 1, \dots, N_y$ we find

$$\|u_h\|_2^2 = \|U_{3h}\|_2^2 + \|Z_h^u\|_2^2. \quad (101)$$

Since similar equalities hold for the other components, we conclude that

$$\|\mathbf{u}_h\|_2^2 = \|\mathbf{U}_{3h}\|_2^2 + \|\mathbf{Z}_h\|_2^2. \quad (102)$$

³ Including, strictly speaking, the separation edges.

For the time discretization we will now proceed to some extent in space dimension one. We define a time step Δt and we are given two integers $p > 1$ and $q > 1$. We will perform p steps with the small time step $\Delta t/p$ and the fine mesh and then we make q steps with the “large” time step Δt and the coarse mesh; and then we start again with the p steps.

3.2.3. The fine grid scheme with small time step

We start from Eq. (95) that we discretize in time thanks to the implicit Euler scheme. This gives

$$\begin{cases} \frac{p}{\Delta t} (u_h^\tau - u_h^{\tau-1/p}) + \tilde{u}_0 \delta_h^x u_h^\tau + \tilde{v}_0 \delta_h^y u_h^\tau + g \delta_h^x \phi_h^\tau = 0, \\ \frac{p}{\Delta t} (v_h^\tau - v_h^{\tau-1/p}) + \tilde{u}_0 \delta_h^x v_h^\tau + \tilde{v}_0 \delta_h^y v_h^\tau + g \delta_h^y \phi_h^\tau = 0, \\ \frac{p}{\Delta t} (\phi_h^\tau - \phi_h^{\tau-1/p}) + \tilde{u}_0 \delta_h^x \phi_h^\tau + \tilde{v}_0 \delta_h^y \phi_h^\tau + \tilde{\phi}_0 (\delta_h^x u_h^\tau + \delta_h^y v_h^\tau) = 0, \end{cases} \tag{103}$$

where $\tau = n + s/p, s = 1, \dots, p$ and $\mathbf{u}_h^\tau = (u_h^\tau, v_h^\tau, \phi_h^\tau)$ is an approximation at time $(n + s/p)\Delta t$.

Let us investigate the stability of this scheme. Recalling our norm on $L^2(\mathcal{M})^3$ given by (92), we aim to estimate

$$\begin{aligned} \|\mathbf{u}_h^\tau\|_2^2 &= \int \int_{\mathcal{M}} u_h^\tau(x, y)^2 dx dy + \int \int_{\mathcal{M}} v_h^\tau(x, y)^2 dx dy + \frac{g}{\phi_0} \\ &\times \int \int_{\mathcal{M}} \phi_h^\tau(x, y) 2 dx dy. \end{aligned} \tag{104}$$

For that purpose, we multiply the equation for u_h^τ by u_h^τ , the one for v_h^τ by v_h^τ , the one for ϕ_h^τ by $\frac{g}{\phi_0} \phi_h^\tau$, integrate over \mathcal{M} and add the corresponding equalities. This provides

$$I_0^h + I_1^h + I_2^h = 0 \tag{105}$$

where

$$\begin{aligned} I_0^h &= \frac{p}{\Delta t} \\ &\times \int \int_{\mathcal{M}} \left[(u_h^\tau - u_h^{\tau-1/p}) u_h^\tau + (v_h^\tau - v_h^{\tau-1/p}) v_h^\tau + \frac{g}{\phi_0} (\phi_h^\tau - \phi_h^{\tau-1/p}) \phi_h^\tau \right] dx dy, \end{aligned} \tag{106}$$

$$I_1^h = \int \int_{\mathcal{M}} \left[\tilde{u}_0 u_h^\tau \delta_h^x u_h^\tau + g u_h^\tau \delta_h^x \phi_h^\tau + \tilde{u}_0 v_h^\tau \delta_h^x v_h^\tau + \frac{g}{\phi_0} \tilde{u}_0 \phi_h^\tau \delta_h^x \phi_h^\tau + g \phi_h^\tau \delta_h^x u_h^\tau \right] dx dy, \tag{107}$$

$$I_2^h = \int \int_{\mathcal{M}} \left[\tilde{v}_0 v_h^\tau \delta_h^y v_h^\tau + g v_h^\tau \delta_h^y \phi_h^\tau + \tilde{v}_0 u_h^\tau \delta_h^y u_h^\tau + \frac{g}{\phi_0} \tilde{v}_0 \phi_h^\tau \delta_h^y \phi_h^\tau + g \phi_h^\tau \delta_h^y v_h^\tau \right] dx dy. \tag{108}$$

For the term I_0^h , using the identity

$$2 \int \int_{\mathcal{M}} (u_h^\tau - u_h^{\tau-1/p}) u_h^\tau dx dy = \int \int_{\mathcal{M}} \left[|u_h^\tau|^2 - |u_h^{\tau-1/p}|^2 + |u_h^\tau - u_h^{\tau-1/p}|^2 \right] dx dy$$

as well as similar ones for the other discrete quantities v_h^τ and ϕ_h^τ , we see that

$$I_0^h = \frac{p}{2\Delta t} (\|\mathbf{u}_h^\tau\|_2^2 - \|\mathbf{u}_h^{\tau-1/p}\|_2^2 + \|\mathbf{u}_h^\tau - \mathbf{u}_h^{\tau-1/p}\|_2^2). \tag{109}$$

We now aim to derive the positivity of I_1^h and I_2^h (which are discrete analogs of $I^1(t)$ and $I^2(t)$ in the proof of Theorem 3). We first remark that

$$\begin{aligned} \int \int_{\mathcal{M}} \tilde{u}_0 u_h^\tau \delta_h^x u_h^\tau dx dy &= \tilde{u}_0 \Delta y \sum_{i=1}^{3N_x} \sum_{j=1}^{3N_y} u_{i,j}^\tau (u_{i,j}^\tau - u_{i-1,j}^\tau) \\ &= \frac{\tilde{u}_0}{2} \Delta y \sum_{i=1}^{3N_x} \sum_{j=1}^{3N_y} \left(|u_{i,j}^\tau|^2 - |u_{i-1,j}^\tau|^2 + |u_{i,j}^\tau - u_{i-1,j}^\tau|^2 \right). \end{aligned} \tag{110}$$

Hence

$$\int \int_{\mathcal{M}} \tilde{u}_0 u_h^\tau \delta_h^x u_h^\tau dx dy = \frac{\tilde{u}_0}{2} \Delta y \sum_{j=1}^{3N_y} \left(|u_{3N_x,j}^\tau|^2 + \sum_{i=1}^{3N_x} |u_{i,j}^\tau - u_{i-1,j}^\tau|^2 \right).$$

Of course, similar identities involving v_h^τ and ϕ_h^τ hold true. Writing also

$$\begin{aligned} (\phi_{i,j}^\tau - \phi_{i-1,j}^\tau) u_{i,j}^\tau + (u_{i,j}^\tau - u_{i-1,j}^\tau) \phi_{i,j}^\tau &= u_{i,j}^\tau \phi_{i,j}^\tau - u_{i-1,j}^\tau \phi_{i-1,j}^\tau \\ &+ (u_{i,j}^\tau - u_{i-1,j}^\tau) (\phi_{i,j}^\tau - \phi_{i-1,j}^\tau), \end{aligned}$$

we obtain

$$\begin{aligned} I_1^h &\geq \frac{\tilde{u}_0}{2} \Delta y \sum_{j=1}^{3N_y} (|u_{3N_x,j}^\tau|^2 + \frac{g}{\phi_0} |\phi_{3N_x,j}^\tau|^2) + \frac{\tilde{u}_0}{2} \Delta y \sum_{i=1}^{3N_x} \sum_{j=1}^{3N_y} |u_{i,j}^\tau - u_{i-1,j}^\tau|^2 \\ &+ \frac{g}{\phi_0} \frac{\tilde{u}_0}{2} \Delta y \sum_{i=1}^{3N_x} \sum_{j=1}^{3N_y} |\phi_{i,j}^\tau - \phi_{i-1,j}^\tau|^2 \\ &+ g \Delta y \sum_{i=1}^{3N_x} \sum_{j=1}^{3N_y} (u_{i,j}^\tau - u_{i-1,j}^\tau) (\phi_{i,j}^\tau - \phi_{i-1,j}^\tau) + g \Delta y \sum_{j=1}^{3N_y} u_{3N_x,j}^\tau \phi_{3N_x,j}^\tau. \end{aligned}$$

Now, since $\tilde{u}_0 > 0$ and $\tilde{u}_0^2 > g\tilde{\phi}_0$, the expressions

$$\frac{\tilde{u}_0}{2} |u_{i,j}^\tau - u_{i-1,j}^\tau|^2 + \frac{\tilde{u}_0}{2} \frac{g}{\phi_0} |\phi_{i,j}^\tau - \phi_{i-1,j}^\tau|^2 + g(u_{i,j}^\tau - u_{i-1,j}^\tau) (\phi_{i,j}^\tau - \phi_{i-1,j}^\tau),$$

and

$$\frac{\tilde{u}_0}{2} |u_{3N_x,j}^\tau|^2 + \frac{\tilde{u}_0}{2} \frac{g}{\phi_0} |\phi_{3N_x,j}^\tau|^2 + g u_{3N_x,j}^\tau \phi_{3N_x,j}^\tau,$$

are positive. Therefore, the corresponding sums are positive and we obtain that $I_1^h \geq 0$. Since the expression for I_2^h is similar to the one for I_1^h , analogous arguments provide $I_2^h \geq 0$.

Coming back to (105), we have $I_0^h = -I_1^h - I_2^h \leq 0$. Recalling (109), this provides

$$\frac{p}{2\Delta t} (\|\mathbf{u}_h^\tau\|_2^2 - \|\mathbf{u}_h^{\tau-1/p}\|_2^2 + \|\mathbf{u}_h^\tau - \mathbf{u}_h^{\tau-1/p}\|_2^2) = -I_1^h - I_2^h \leq 0,$$

so that

$$\|\mathbf{u}_h^\tau\|_2^2 \leq \|\mathbf{u}_h^{\tau-1/p}\|_2^2. \tag{111}$$

Since $\tau = n + s/p$, this yields for $s = 1, \dots, p$:

$$\|\mathbf{u}_h^{n+s/p}\|_2 \leq \|\mathbf{u}_h^n\|_2, \tag{112}$$

so that the p steps of the scheme (103) on the fine grid are stable.

3.2.4. The coarse grid scheme with large time step

We now consider the q time-steps performed on the coarse grid with time step Δt . The scheme is obtained by discretizing (99) with respect to time thanks to the implicit Euler scheme. It reads:

$$\begin{cases} \frac{1}{\Delta t} (U_{3h}^\tau - U_{3h}^{\tau-1}) + \tilde{u}_0 \delta_{3h}^x U_{3h}^\tau + \tilde{v}_0 \delta_{3h}^y U_{3h}^\tau + g \delta_{3h}^x \Phi_{3h}^\tau = 0, \\ \frac{1}{\Delta t} (V_{3h}^\tau - V_{3h}^{\tau-1}) + \tilde{u}_0 \delta_{3h}^x V_{3h}^\tau + \tilde{v}_0 \delta_{3h}^y V_{3h}^\tau + g \delta_{3h}^y \Phi_{3h}^\tau = 0, \\ \frac{1}{\Delta t} (\Phi_{3h}^\tau - \Phi_{3h}^{\tau-1}) + \tilde{u}_0 \delta_{3h}^x \Phi_{3h}^\tau + \tilde{v}_0 \delta_{3h}^y \Phi_{3h}^\tau + \tilde{\phi}_0 (\delta_{3h}^x U_{3h}^\tau + \delta_{3h}^y V_{3h}^\tau) = 0, \end{cases} \tag{113}$$

where $\tau = n + s + 1, s = 1, \dots, q, \mathbf{U}_h^\tau = (U_{3h}^\tau, V_{3h}^\tau, \Phi_{3h}^\tau)$.

This scheme is similar to (103) and as in Section 3.2.3 we can derive that

$$\frac{1}{2\Delta t} (\|\mathbf{U}_{3h}^\tau\|_2^2 - \|\mathbf{U}_{3h}^{\tau-1}\|_2^2 + \|\mathbf{U}_{3h}^\tau - \mathbf{U}_{3h}^{\tau-1}\|_2^2) \leq 0,$$

hence

$$\|\mathbf{U}_{3h}^{n+s+1}\|_2 \leq \|\mathbf{U}_{3h}^{n+1}\|_2. \tag{114}$$

During the steps from $(n+1)\Delta t$ to $(n+q+1)\Delta t$, the \mathbf{Z}_h are frozen, thus

$$\mathbf{Z}_h^{n+s+1} = \mathbf{Z}_h^{n+1}, s = 1, \dots, q, \quad (115)$$

and we recover the \mathbf{u}_h^{n+s+1} in the form

$$\mathbf{u}_h^{n+s+1} = \mathbf{U}_{3h}^{n+s+1} + \mathbf{Z}_h^{n+1}. \quad (116)$$

Then, thanks to (102):

$$\|\mathbf{u}_h^{n+s+1}\|_2^2 = \|\mathbf{U}_{3h}^{n+s+1}\|_2^2 + \|\mathbf{Z}_h^{n+1}\|_2^2.$$

Finally, combining with (114) and using (102) again, we conclude that

$$\|\mathbf{u}_h^{n+s+1}\|_2^2 \leq \|\mathbf{U}_{3h}^{n+1}\|_2^2 + \|\mathbf{Z}_h^{n+1}\|_2^2 = \|\mathbf{u}_h^{n+1}\|_2^2, \quad (117)$$

so that

$$\|\mathbf{u}_h^{n+s+1}\|_2 \leq \|\mathbf{u}_h^{n+1}\|_2. \quad (118)$$

Theorem 4. *The multilevel scheme defined by the Eqs. (103), (113) and (116) is stable in the L^2 norm given by (92). More precisely, for all n and $r \geq 0$:*

$$\begin{aligned} \|\mathbf{u}_h^n\|_2 &\leq \|\mathbf{u}^0\|_2, \\ \|\mathbf{u}_h^{r(q+1)+s/p}\|_2 &\leq \|\mathbf{u}^0\|_2, \quad \text{for } s = 1, \dots, p. \end{aligned} \quad (119)$$

3.3. Conclusion

An attempt has been made at studying the stability of the schemes derived from the Finite Volume Incremental Unknowns (FVIU) method using the tools of numerical analysis. The issue is much more complex than one might think. At this time several issues remain open, e.g. the study of the stability of the FVIU method presented in Part I and implemented in our numerical simulations; this method uses increments \mathbf{Z} of order $(\Delta x)^2$, where Δx is the mesh size. We were able in Part II to study the stability of two versions of the FVIU method, both with increments of order Δx . For one of the methods, we were able to study the stability of the scheme in space dimension 2 (see [12] for space dimension one). For another version of the method which we believe more “natural” we proved the stability for the one dimensional problem using the von Neumann stability method, but the study of the stability using energy methods or in space dimension two remains open.

Beside these intriguing questions in numerical analysis, there is the major issue of the boundary conditions on the fine grid when using multi-level methods, which we addressed in a simplified way in [1] and in Part I of this article. We intend to study this problem more thoroughly in a future work but, at this point, we now turn, in Part III, to the issue of the boundary conditions.

4. Part III: Boundary conditions for the shallow water equations

Part III of this article is devoted to the issue of boundary conditions. We will consider the nonlinear shallow water equations in a rectangle \mathcal{M} as in Part I and, for the numerical simulations, we will focus on some variations of a classical test problem in oceanography, namely the Rossby equatorial soliton. Boundary conditions are proposed which are expected to lead to a well posed problem; see some partial results in the mathematical literature in [46–48,34,32,33]. Further numerical exploration of these boundary conditions appear in [13]. The issue of the boundary conditions is discussed in the physical context in e.g. the Refs. [7,9,27,28,31,40,43–45,50,54,55,57,58]. Note that, as indicated in the

general introduction, the issue of the boundary conditions is present in the multilevel methods (in general) in relation with the passage of information between the large cells and the small cells; such question will be studied elsewhere.

The choice of the boundary conditions for problems arising from the geophysical fluid dynamics is very important, especially when the problem is considered on a limited domain (limited area model). The difficulty in this context consists in the fact that the physical domain is too large in order to allow us to compute numerically the solution of the problem directly on it, so we are obliged to decompose the domain into several smaller subdomains and to compute the solution on these subdomains which do not have in general a physical significance. Therefore, on these subdomains there are no physical laws which can provide the conditions at the boundary. Thus, the choice of the boundary conditions must be based on other considerations such as the physical intuition and the numerical relevance. Since the shallow water equations form an hyperbolic system, the direction of the characteristics at the boundary will provide us important valuable information, the idea being to propose boundary conditions that allow the waves to enter and leave freely the computational domain without generating undesirable reflections at the boundary. In the mathematical literature such boundary conditions are called *transparent boundary conditions*. In what follows we consider such boundary conditions and we know the problem is well-posed for the one-dimensional shallow water equations and numerically we will see that no artificial reflexions at the boundary appear, contrary to the case when the Dirichlet boundary conditions are considered.

4.1. Shallow water equations in a rectangle: equations and boundary conditions

The two-dimensional nonlinear inviscid shallow water equations will be considered in two different forms. To derive the suitable boundary conditions, we consider the original variables u, v, ϕ representing the two-components of the velocity and the height, and the equations read

$$\begin{cases} \frac{\partial u}{\partial t} + u \frac{\partial u}{\partial x} + v \frac{\partial u}{\partial y} + g \frac{\partial \phi}{\partial x} - f v = 0, \\ \frac{\partial v}{\partial t} + u \frac{\partial v}{\partial x} + v \frac{\partial v}{\partial y} + g \frac{\partial \phi}{\partial y} + f u = 0, \\ \frac{\partial \phi}{\partial t} + \frac{\partial u \phi}{\partial x} + \frac{\partial v \phi}{\partial y} = 0, \end{cases} \quad (120)$$

considered on the rectangular domain $\mathcal{M} = (0, L_x) \times (0, L_y)$.

For the actual simulations, we will, as in Part I, consider the shallow water equations in the conservative form in which the variables are $\mathbf{u} = (u, v, \phi)$, $u = u\phi$ and $v = v\phi$:

$$\begin{cases} \frac{\partial u \phi}{\partial t} + \frac{\partial \phi u^2}{\partial x} + \frac{\partial \phi u v}{\partial y} + \frac{g}{2} \frac{\partial \phi^2}{\partial x} - f v \phi = 0, \\ \frac{\partial v \phi}{\partial t} + \frac{\partial \phi u v}{\partial x} + \frac{\partial \phi v^2}{\partial y} + \frac{g}{2} \frac{\partial \phi^2}{\partial y} + f u \phi = 0, \\ \frac{\partial \phi}{\partial t} + \frac{\partial u \phi}{\partial x} + \frac{\partial v \phi}{\partial y} = 0. \end{cases} \quad (121)$$

The only difference with (1) is the introduction of the Coriolis force $(-f v \phi, f u \phi, 0)$.

Boundary conditions

In our numerical study, we will associate two types of boundary conditions to Eqs. (120) and (121);

- The Dirichlet boundary conditions for which we prescribe u, v, ϕ at the boundary (see below for the Rossby soliton), denoted $u_{\partial \mathcal{M}}, v_{\partial \mathcal{M}}, \phi_{\partial \mathcal{M}}$.
- The transparent boundary conditions which we now describe.

For the transparent boundary conditions we have a different set of boundary conditions on different parts of the boundary. These boundary conditions are not applied on the unknowns u, v, ϕ but

on suitable combinations of these unknowns for the West and East boundaries. They are defined as follows:

$$\text{West, East} \begin{cases} \alpha = \frac{u}{2} - \sqrt{gh}\phi, \\ \alpha = v, \\ \alpha = \frac{u}{2} + \sqrt{gh}\phi. \end{cases} \quad (122)$$

First we remark, using (120), that α, β and γ are solutions of the following system:

$$\begin{cases} \frac{\partial \alpha}{\partial t} + \frac{3\alpha + \gamma}{2} \frac{\partial \alpha}{\partial x} - \frac{\gamma - \alpha}{4} \frac{\partial \beta}{\partial y} + \beta \frac{\partial \alpha}{\partial y} - \frac{f\beta}{2} = 0, \\ \frac{\partial \beta}{\partial t} + \frac{\partial \beta}{\partial x} (\alpha + \gamma) - \beta \frac{\partial \beta}{\partial y} + \frac{\gamma - \alpha}{8} \frac{\partial (\beta - \alpha)}{\partial y} + f(\alpha + \gamma) = 0, \\ \frac{\partial \gamma}{\partial t} + \frac{\alpha + 3\gamma}{2} \frac{\partial \gamma}{\partial x} + \frac{\gamma - \alpha}{4} \frac{\partial \beta}{\partial y} + \beta \frac{\partial \gamma}{\partial y} - \frac{f\beta}{2} = 0. \end{cases} \quad (123)$$

With these variables the transparent boundary conditions that we propose are, for the East boundary, Dirichlet boundary conditions for α . These conditions hence read:

$$\alpha = \alpha_{\partial \mathcal{M}}, \quad (124)$$

where $\alpha_{\partial \mathcal{M}} = u_{\partial \mathcal{M}}/2 - \sqrt{gh}\phi_{\partial \mathcal{M}}$, and $u_{\partial \mathcal{M}}, v_{\partial \mathcal{M}}, \phi_{\partial \mathcal{M}}$ given (see below for the Rossby soliton).

For the West boundary we use a Dirichlet boundary condition for β and γ . Hence:

$$\begin{cases} \beta = \beta_{\partial \mathcal{M}}, \\ \gamma = \gamma_{\partial \mathcal{M}}, \end{cases} \quad (125)$$

where $\gamma_{\partial \mathcal{M}} = u_{\partial \mathcal{M}}/2 + \sqrt{gh}\phi_{\partial \mathcal{M}}, \beta_{\partial \mathcal{M}} = v_{\partial \mathcal{M}}$ and $u_{\partial \mathcal{M}}, v_{\partial \mathcal{M}}$ and $\phi_{\partial \mathcal{M}}$ given.

For the North and South boundaries we use the Dirichlet boundary conditions because we assume that our wave, the Rossby soliton, does not go out or from these boundaries. For the Rossby soliton, the wave travels from West to East; there is almost no activity on the North and South boundary. If the wave travels also in the North–South direction, we would have to consider similar unknowns where u and v would be swapped.

Once we know α, β and γ on the boundary (or on a fictitious cell) we can then find the values of our unknowns u, v and ϕ by inverting the system (122).

In what follows, we give some more details related to the choice of the transparent boundary conditions. We first mention here that the choice of the transparent boundary conditions is related to the nature of the flow. We thus distinguish between the subcritical flows, for which $u^2 < gh$, and the supercritical flows, for which $u^2 > gh$. The importance of this distinction will become clear hereafter. For the subcritical flows, the boundary conditions are given as follows:

$$\begin{aligned} \alpha(0, y, t) &:= u(0, y, t) + 2\sqrt{gh(0, y, t)} = \alpha_{\partial \mathcal{M}}, \\ \beta(0, y, t) &:= v(0, y, t) = \beta_{\partial \mathcal{M}}, \\ \gamma(L_x, y, t) &:= u(L_x, y, t) - 2\sqrt{gh(L_x, y, t)} = \gamma_{\partial \mathcal{M}}, \end{aligned} \quad (126)$$

and for the supercritical flows the boundary conditions are given as follows:

$$\begin{aligned} \alpha(0, y, t) &:= u(0, y, t) + 2\sqrt{gh(0, y, t)} = \alpha_{\partial \mathcal{M}}, \\ \beta(0, y, t) &:= v(0, y, t) = \beta_{\partial \mathcal{M}}, \\ \gamma(0, y, t) &:= u(0, y, t) - 2\sqrt{gh(0, y, t)} = \gamma_{\partial \mathcal{M}}, \end{aligned} \quad (127)$$

where $\alpha_{\partial \mathcal{M}}, \beta_{\partial \mathcal{M}}, \gamma_{\partial \mathcal{M}}$ are given.

The choice of these transparent boundary conditions and the relation between these boundary conditions and system (122) given in terms of the unknowns α, β and γ is natural. In fact, we first write problem (120) in the matrix form:

$$U_t + A(U)U_x + B(U)U_y + CU = 0, \quad (128)$$

where U is the vector formed by the unknowns (u, v, ϕ) and the matrices $A(U), B(U), C$ are given by:

$$A(U) = \begin{pmatrix} u & 0 & g \\ 0 & u & 0 \\ \phi & 0 & u \end{pmatrix}, \quad B(U) = \begin{pmatrix} v & 0 & 0 \\ 0 & v & g \\ \phi & 0 & v \end{pmatrix}, \quad C = \begin{pmatrix} 0 & -f & 0 \\ f & 0 & 0 \\ 0 & 0 & 0 \end{pmatrix}. \quad (129)$$

Since for the Rossby soliton considered here, the wave moves from West to East, we compute the eigenvalues of the matrix $A(U)$. We find:

$$\lambda_1 = u - \sqrt{gh}, \quad \lambda_2 = u, \quad \lambda_3 = u + \sqrt{gh}, \quad (130)$$

and we analyse the sign of the eigenvalues.

Performing linear combinations $(\pm\sqrt{g/h}, 1)$ between the first and the last lines of system (120), we find:

$$\begin{cases} \frac{\partial}{\partial t} (\frac{u}{2} - \sqrt{gh}) + \lambda_1 \frac{\partial}{\partial x} (\frac{u}{2} - \sqrt{gh}) + \dots = 0, \\ \frac{\partial v}{\partial t} + \lambda_2 \frac{\partial v}{\partial x} + v \frac{\partial v}{\partial y} + \dots = 0, \\ \frac{\partial}{\partial t} (\frac{u}{2} + \sqrt{gh}) + \lambda_3 \frac{\partial}{\partial x} (\frac{u}{2} + \sqrt{gh}) + \dots = 0, \end{cases} \quad (131)$$

which is exactly system (123) written in terms of the new variables α, β and γ . Thus, we can consider that the Rossby soliton satisfies, in the x -direction, three transport equations given in terms of the characteristic unknowns α, β and γ . The boundary conditions are imposed accordingly to the sign of the eigenvalues λ_1, λ_2 and λ_3 and this is the reason for which we distinguish between the subcritical case $u^2 - gh < 0$ for which $\lambda_1 < 0, \lambda_2 > 0, \lambda_3 > 0$ and the supercritical case $u^2 - gh > 0$ for which $\lambda_1 > 0, \lambda_2 > 0, \lambda_3 > 0$.

For the subcritical case, we need to impose a boundary condition on α at the exit of the domain (thus, on the East boundary condition) and two boundary conditions at the entrance of the domain by prescribing β and γ on the West boundary. This is the scenario for the Rossby soliton that we consider in the numerical tests, that is why we consider the boundary conditions (124) and (125).

For the supercritical flows, all the characteristic variables are entering the domain and we need to prescribe α, β and γ on the West boundary.

If the wave travels in the North–South direction, the same analysis is applied but to the matrix $B(U)$. In this case, the eigenvalues of the $B(U)$ matrix are $v - \sqrt{gh}, v$ and $v + \sqrt{gh}$ and the characteristic unknowns are $v/2 - \sqrt{gh}, v$ and $v/2 + \sqrt{gh}$.

4.2. The Rossby soliton

The equations are slightly different than the usual shallow water equations because we add the Coriolis force. Furthermore, we consider two different boundary conditions: the Dirichlet boundary conditions and the transparent conditions. The test model considered in the geophysical literature is described in details at this address: <http://marine.rutgers.edu/po/tests/rossby/index.html>, and it corresponds to the Dirichlet boundary conditions.

We use a finite volume method to solve this system of equations, and to be specific we use the central-upwind scheme; see [1].

The equations and all quantities being non-dimensional, we consider the flow in the domain

$$\mathcal{M} = (-24, 24) \times (-8, 8),$$

over the interval of time $0 < t < T$. We have:

$$\frac{\partial \mathbf{u}}{\partial t} + \frac{\partial F(\mathbf{u})}{\partial x} + \frac{\partial G(\mathbf{v})}{\partial y} = \mathbf{S}, \quad (132)$$

where

$$\mathbf{u} = \begin{pmatrix} u \\ v \\ \phi \end{pmatrix}, \quad F(\mathbf{u}) = \begin{pmatrix} \frac{u^2}{\phi} + \frac{g\phi^2}{2} \\ \frac{uv}{\phi} \\ u \end{pmatrix}, \quad G(\mathbf{u}) = \begin{pmatrix} \frac{uv}{\phi} \\ \frac{v^2}{\phi} + \frac{g\phi^2}{2} \\ v \end{pmatrix}.$$

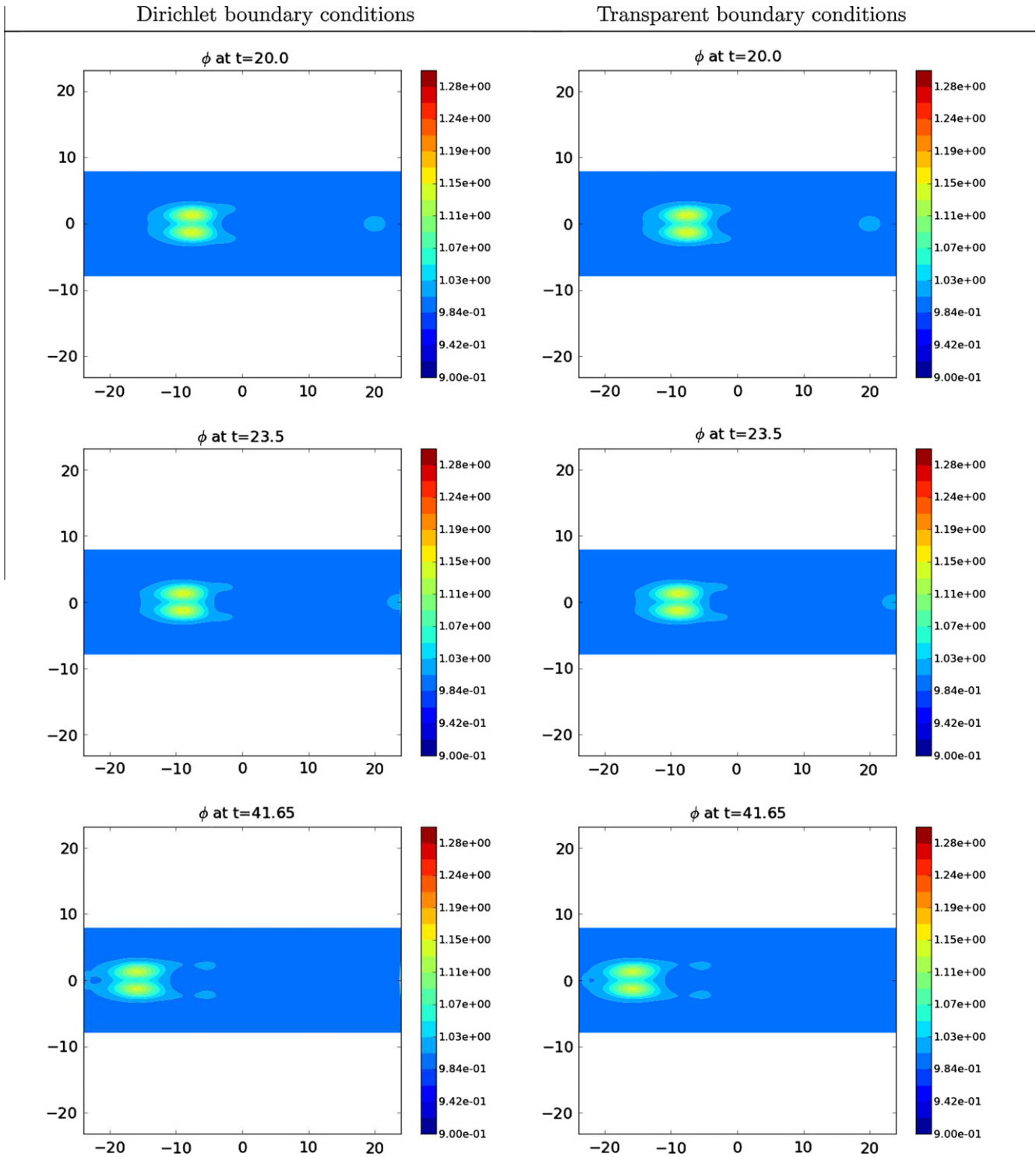


Fig. 18. Evolution of the Rossby soliton at the indicated times (20, 23.5, 41.65), left column: Dirichlet boundary condition, right column: transparent boundary condition.

The only difference now, compared to Part I, is the introduction of the Coriolis force denoted by \mathbf{S} (which is not really a source term but will be treated as such in the numerical simulations).

We have the following constants:

- g denotes the gravity, in this case $g = 1$
- f is the Coriolis force, which is equal to $f_0 + \bar{f}y$, in this case $f_0 = 0$ and $\bar{f} = 1$

The initial data are the following:

$$\begin{cases} u(x, y, 0) = \phi(x) \frac{(-9+6y^2)}{4} e^{-\frac{y^2}{2}}, \\ v(x, y, 0) = \frac{\partial \phi(x)}{\partial x} (2y) e^{-\frac{y^2}{2}}, \\ h(x, y, 0) = \psi(x) \frac{(3+6y^2)}{4} e^{-\frac{y^2}{2}} + 1, \end{cases} \quad (133)$$

with:

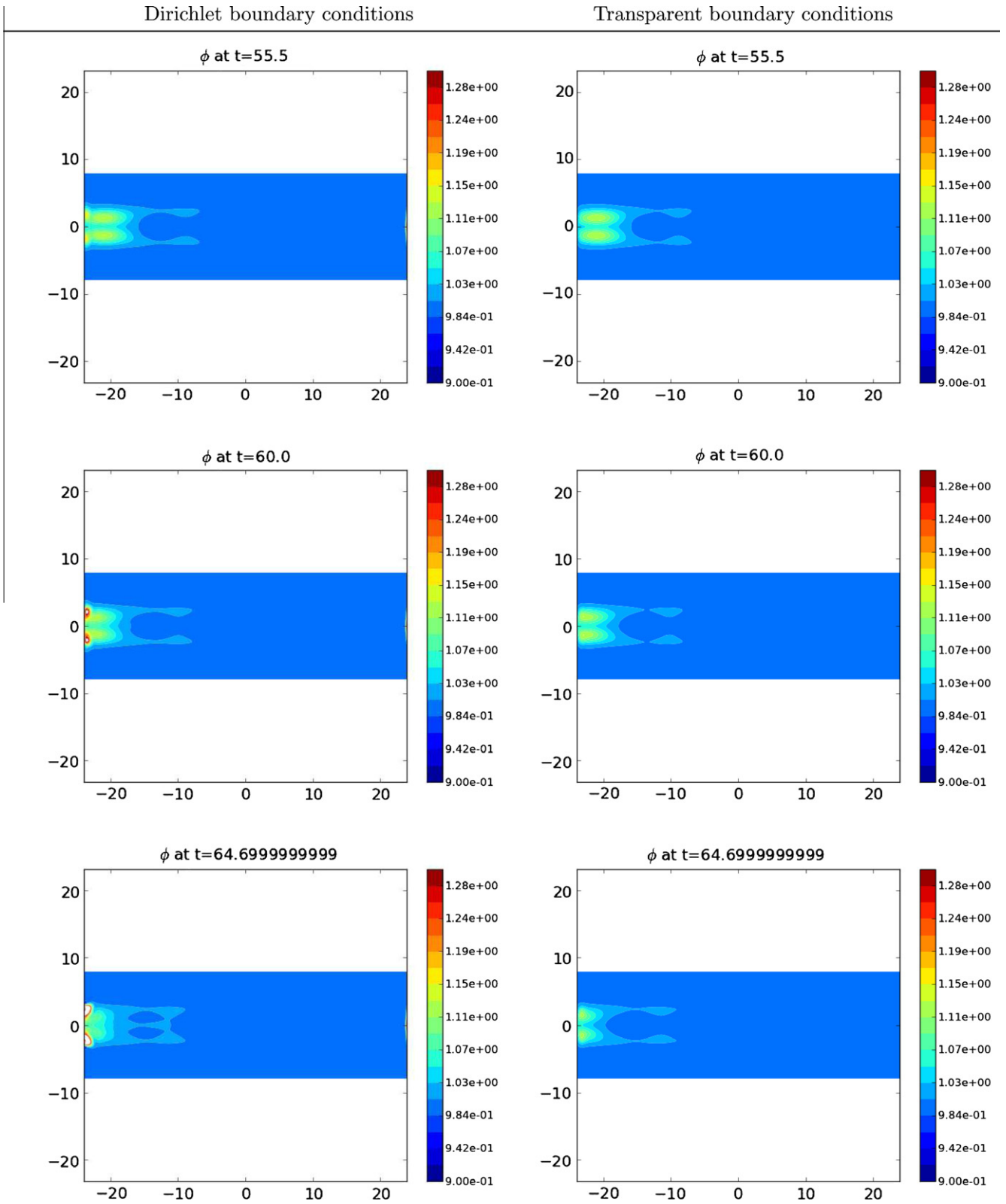


Fig. 19. Evolution of the Rossby soliton at the indicated times (55.5, 60, 64.7), left column: Dirichlet boundary condition, right column: transparent boundary condition.

$$\begin{aligned}
 B &= 0.395, \\
 A &= 0.7771B^2, \\
 \psi(x) &= A \operatorname{sech}^2 Bx, \\
 \frac{\partial \phi(x)}{\partial x} &= -2B \tanh(Bx) \phi.
 \end{aligned}$$

The Dirichlet boundary conditions all over $\partial \mathcal{M}$ read:

$$\begin{cases}
 u_{\partial \mathcal{M}} = 0, \\
 v_{\partial \mathcal{M}} = 0, \\
 \phi_{\partial \mathcal{M}} = 1.
 \end{cases} \tag{134}$$

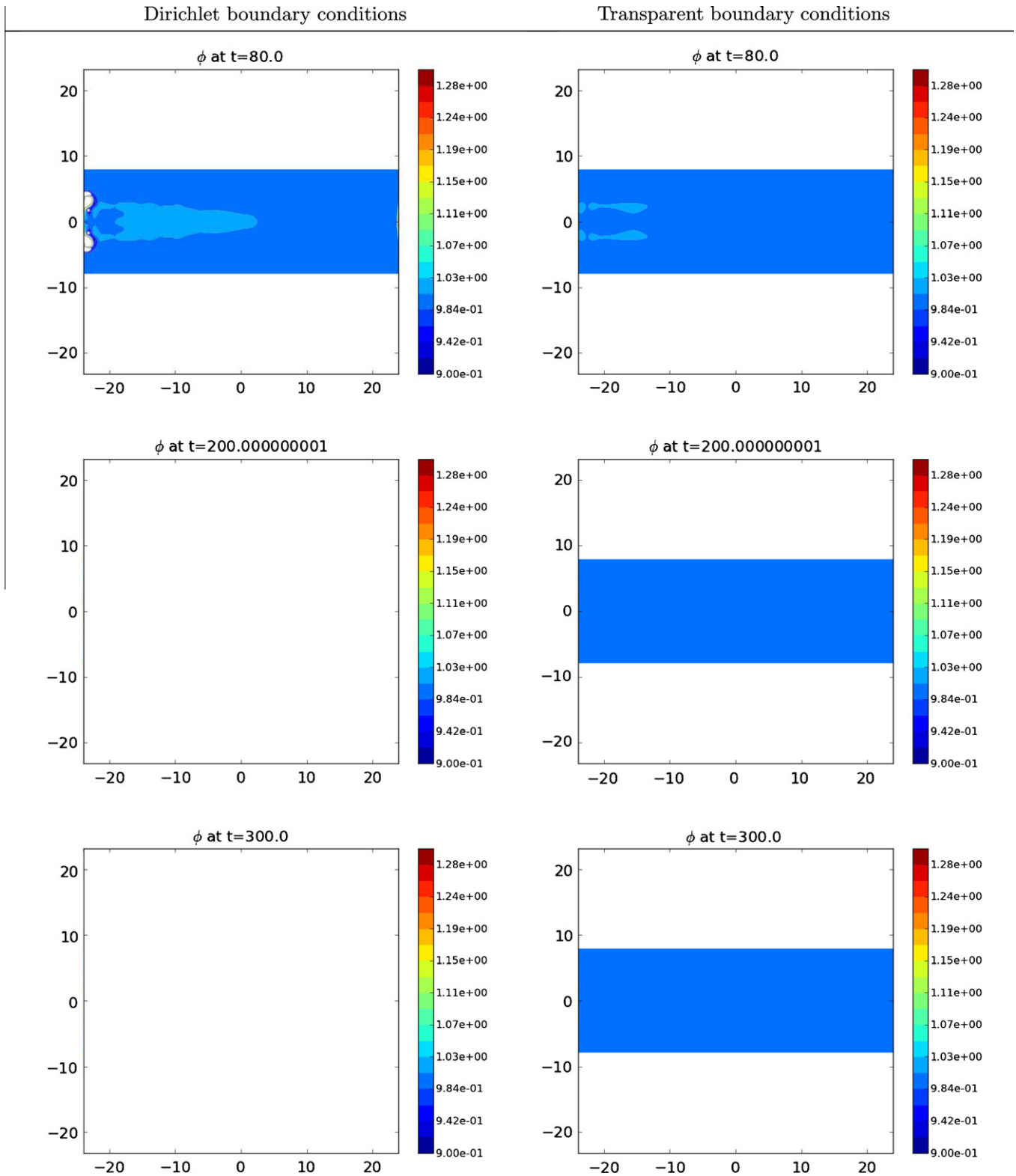


Fig. 20. Evolution of the Rossby soliton at the indicated times (80, 200, 300), left column: Dirichlet boundary condition, right column: transparent boundary condition.

4.3. The numerical procedure

The discretization of the domain \mathcal{A} is done using rectangular finite volumes $K_m = [x_{m/w}, x_{m/e}] \times [y_{m/s}, y_{m/n}]$ of centers (x_m, y_m) and of size $\Delta x \times \Delta y$, where N_x, N_y are two integers such that $N_x \Delta x = L_x$ and $N_y \Delta y = L_y$.

The unknowns will be approximations of the cell averages:

$$\mathbf{u}_m(t) = \frac{1}{\Delta x \Delta y} \int_{K_m} \mathbf{u}(x, y, t) dx dy,$$

where $\mathbf{u}_m(t) = (u_m(t), v_m(t), \phi_m(t))$.

In order to obtain the discretized equations, we integrate the system (132) on each cell K_m and we divide by its area $\Delta x \Delta y$; we find

$$\frac{d}{dt} \mathbf{u}_m(t) = - \frac{H_{m/e}^x(t) - H_{w/m}^x(t)}{\Delta x} - \frac{H_{m/n}^y(t) - H_{s/m}^y(t)}{\Delta y}. \quad (135)$$

The fluxes $H_{m/e}^x(t)$ and $H_{m/n}^y(t)$ are respectively the East flux (along the x axis) and the North flux (along the y axis) on the edges between K_m and K_e , and between K_m and K_n , see Fig. 3. The other fluxes are defined similarly.

We write one of the fluxes explicitly:

$$H_{m/e}^x(t) = \frac{1}{\Delta x} \int_{\Gamma_{m/e}} F(\mathbf{u}(t, x, y)) dy.$$

The approximation of the fluxes is done using a semi-discrete central-upwind scheme exactly as in Part I, Eqs. (9)–(12).

These definitions of the fluxes are valid for the volumes inside \mathcal{M} . For the cells at the boundary of our mesh we have to define fictitious cells. In each case we have:

- If “n” does not exist:

$$H_{m/n}^y = G(\mathbf{u}_{\partial \mathcal{M}}^N)$$

- If “s” does not exist:

$$H_{s/m}^y = G(\mathbf{u}_{\partial \mathcal{M}}^S)$$

- If “e” does not exist:

$$H_{m/e}^x = F(\mathbf{u}_{\partial \mathcal{M}}^E)$$

- If “w” does not exist:

$$H_{w/m}^x = F(\mathbf{u}_{\partial \mathcal{M}}^W)$$

In the case of Dirichlet boundary conditions we take:

$$u_{\partial \mathcal{M}}^N = u_{\partial \mathcal{M}}^S = u_{\partial \mathcal{M}}^E = u_{\partial \mathcal{M}}^W = u_{\partial \mathcal{M}} = 0,$$

$$v_{\partial \mathcal{M}}^N = v_{\partial \mathcal{M}}^S = v_{\partial \mathcal{M}}^E = v_{\partial \mathcal{M}}^W = v_{\partial \mathcal{M}} = 0,$$

$$\phi_{\partial \mathcal{M}}^N = \phi_{\partial \mathcal{M}}^S = \phi_{\partial \mathcal{M}}^E = \phi_{\partial \mathcal{M}}^W = \phi_{\partial \mathcal{M}} = 1.$$

In the case of transparent boundary conditions the value of u , v and ϕ on the West, East boundaries are computed using the unknowns α , β , γ . On the East boundary we know the value of α and to compute the value of β and γ we use the Runge–Kutta scheme on the discrete version of (123) for $i = N_x + 1, i = N_x + 2$ and $1 \leq j \leq N_y$:

$$\begin{cases} \frac{\partial \alpha_{ij}^{n+1}}{\partial t} + \frac{\beta_{ij}^n - \beta_{i-1,j}^n}{\Delta x} (\alpha_{ij}^n + \gamma_{ij}^n) - \beta_{ij}^n \frac{\beta_{ij}^n - \beta_{i-1,j}^n}{\Delta y} + \frac{\gamma_{ij}^n - \alpha_{ij}^n}{8} \left(\frac{\alpha_{ij}^n - \alpha_{i,j-1}^n}{\Delta y} - \frac{\gamma_{ij}^n - \gamma_{i,j-1}^n}{\Delta y} \right) \\ + f_{ij}^n (\alpha_{ij}^n + \gamma_{ij}^n) = 0, \\ \frac{\partial \gamma_{ij}^{n+1}}{\partial t} + \frac{\alpha_{ij}^n + 3\gamma_{ij}^n}{2} \frac{\gamma_{ij}^n - \gamma_{i-1,j}^n}{\Delta x} + \frac{\gamma_{ij}^n - \alpha_{ij}^n}{4} \frac{\beta_{ij}^n - \beta_{i-1,j}^n}{\Delta y} + \beta_{ij}^n \frac{\gamma_{ij}^n - \gamma_{i,j-1}^n}{\Delta y} - \frac{f_{ij}^n}{2} = 0. \end{cases} \quad (136)$$

On the West boundary we know the value of β and γ and to compute the value of α we use the Runge–Kutta scheme on the discrete version of (123) for $i = -1, i = -2$ and $1 \leq j \leq N_y$:

$$\begin{aligned} \frac{\partial \alpha_{ij}^{n+1}}{\partial t} + \frac{3\alpha_{ij}^n + \gamma_{ij}^n}{2} \frac{\alpha_{i+1,j}^n - \alpha_{ij}^n}{\Delta x} - \frac{\gamma_{ij}^n - \alpha_{ij}^n}{4} \frac{\beta_{ij}^n - \beta_{i,j-1}^n}{\Delta y} + \beta_{ij}^n \frac{\alpha_{ij}^n - \alpha_{i,j-1}^n}{\Delta y} \\ - \frac{f_{ij}^n}{2} = 0. \end{aligned} \quad (137)$$

As for the boundary conditions on the South and North boundaries we use the Dirichlet boundary conditions on u , v and ϕ because in our case, for the considered soliton, the wave moves from East to West.

The space scheme being now defined, for the time scheme we use a fourth order the Runge–Kutta method defined in Part I.

4.4. Numerical results

The results of the numerical simulations are displayed in Figs. 18 and 19, for the Dirichlet boundary conditions in the left columns, and for the transparent conditions in the right columns. As expected, the behavior of the soliton is essentially the same in both cases until the soliton reaches the boundary at time $t = 41.65$. Then the behaviors are dramatically different with high values of ϕ appearing at both the left and right boundaries ($x = \pm 24$) for the Dirichlet boundary condition. Note, at time $t = 64.69$, the important reflected wave on the left while in the right column the soliton leaves the domain without reflexion at all. Fig. 20 shows that after $t \simeq 65$, the calculations with the Dirichlet condition are not valid anymore, giving an indication that the solution blows up, and that the shallow water equations are not well posed with the Dirichlet boundary conditions (134). On the contrary, in the right column the soliton continues to leave smoothly the domain until it has completely disappeared at time $t = 300$.

4.5. Conclusion

New boundary conditions have been proposed for the inviscid shallow water equations in space dimension one and two and studied in [13]. Fully (in 1D) or partly (in 2D) supported by theoretical studies, these boundary conditions are shown to be “transparent” in our numerical simulations, that is they let the waves move freely out of the domain. The numerical tests relate to the classical equatorial Rossby soliton. The form of these boundary conditions were given in Part III of this article and were numerically implemented in this test problem. Without any attempt at systematic comparison with other open boundary conditions, it is observed that the classical equatorial Rossby soliton with Dirichlet boundary conditions leads to undesirable reflexions when the soliton reaches the boundary, and eventually to numerical blow-up, whereas the proposed boundary conditions let the soliton move freely out of the domain. This issue of the boundary conditions is also addressed in the related reference [13] for two layers of fluid in space dimension one and for other situations in space dimension two.

Acknowledgments

This work was supported in part by the NSF Grants DMS 0906440 and DMS 1206438, and by the Research Fund of Indiana University.

References

- [1] Adamy K, Bousquet A, Faure S, Laminie J, Temam R. A multilevel method for finite volume discretization of the two-dimensional nonlinear shallow water equations. *Ocean Modell* 2010;33(3–4):235–56.
- [2] Alcrudo F, Garcia-Navarro P. A high-resolution Godunov-type scheme in finite volumes for the 2D shallow water equations. *Int J Numer Methods Fluids* 1993;16(6):489–505.
- [3] Audusse E. A multilayer Saint-Venant system: derivation and numerical validation. *Discrete Contin Dyn Syst Ser B* 2005;5:189–214.
- [4] Audusse E, Bouchut F, Bristeau M-O, Klein R, Perthame B. A fast and stable well-balanced scheme with hydrostatic reconstruction for shallow water flows. *SIAM J Sci Comput* 2004;25(6):2050–65.
- [5] Audusse E, Bristeau MO, Klein R, Perthame B. Kinetic schemes for Saint-Venant equations with source terms on unstructured grids INRIA Report RR-3989; 2000.
- [6] Bellanger M. *Traitement du signal*. Dunod, Paris; 2006.
- [7] Bennett AF, Chua BS. Open boundary conditions for Lagrangian geophysical fluid dynamics. *J Comput Phys* 1999;153(2):418–36.
- [8] Benzi-Gavage S, Serre D. *Multidimensional hyperbolic partial differential equations. First-order systems and applications*. Oxford mathematical monographs. Oxford: The Clarendon Press, Oxford University Press; 2007.

- [9] Blayo E, Debreu L. Revisiting open boundary conditions from the point of view of characteristic variables. *Ocean Modell* 2005;9:231–52.
- [10] Bouchut F, Zeitlin V. A robust well-balanced scheme for multi-layer shallow water equations. *DCDS-B* 2010;13(4):739–58.
- [11] Bousquet A, Marion M, Temam R. Finite volume multilevel approximation of the shallow water equations I. *Chinese Annals of Mathematics*; in press.
- [12] Bousquet A, Marion M, Temam R. Finite volume multilevel approximation of the shallow water equations II; in preparation.
- [13] Bousquet A, Petcu M, Shiue MC, Temam R, Tribbia J. Finite volume multilevel boundary conditions for limited area models based on the shallow water equations. *Commun Comput Phys (CICP)*; in press.
- [14] Calgari C, Laminie J, Temam R. Dynamical multilevel schemes for the solution of evolution equations by hierarchical finite element discretization. *Appl Numer Math* 1997;23(4):403–42.
- [15] Canuto C, Hussaini MY, Quarteroni A, Zang TA. Spectral methods. Evolution to complex geometries and applications to fluid dynamics. Scientific computation. Berlin: Springer; 2007.
- [16] Chen M, Temam R. Incremental unknowns in finite differences: condition number of the matrix. *SIAM J Matrix Anal Appl* 1993;14(2):432–55.
- [17] Chen Q, Shiue MC, Temam R. The barotropic mode for the primitive equations. Special issue in memory of David Gottlieb. *J Sci Comput* 2010;45:167–99. doi:10.1007/s10915-009-9343-8. SpringerLink.
- [18] Chen Q, Shiue M-C, Temam R, Tribbia J. Numerical approximation of the inviscid 3D Primitive equations in a limited domain. *Math Mod Numer Anal (M2AN)* 2012;45:619–46. doi:10.105/m2an/2011058.
- [19] Chung TJ. Computational fluid dynamics. Cambridge University Press; 2002.
- [20] Cullen MJP. Analysis of the semi-geostrophic shallow water equations. *Physica D* 2008;237:1461–5.
- [21] Debussche A, Laminie J, Zahrouni E. A dynamical multi-level scheme for the Burgers equation: wavelet and hierarchical finite element. *J Sci Comput* 2005;25(3):445–97.
- [22] Debreu L, Blayo E. Two-way embedding algorithms: a review. *Ocean Dyn* 2008;58:415–28.
- [23] Dubois T, Jauberteau F, Temam R. Dynamic multilevel methods and the numerical simulation of turbulence. Cambridge: Cambridge University Press; 1999.
- [24] Dautray R, Lions JL. Mathematical analysis and numerical methods for science and technology. Berlin: Springer-Verlag; 1990–1992.
- [25] Dubois T, Jauberteau F, Temam R. Incremental unknowns, multilevel methods and the numerical simulation of turbulence. *Comput Methods Appl Mech Eng* 1998;159(1–2):123–89.
- [26] Dubois T, Jauberteau F, Temam R, Tribbia J. Multilevel schemes for the shallow water equations. *J Comput Phys* 2005;207(2):660–94.
- [27] Engquist B, Halpern L. Far field boundary conditions for computation over long time. *Appl Numer Math* 1988;4(1):21–45.
- [28] Engquist B, Majda A. Absorbing boundary conditions for the numerical simulation of waves. *Math Comput* 1977;31(139):629–51.
- [29] Faure S, Laminie J, Temam R. Finite volume discretization and multilevel methods in flow problems. *J Sci Comput* 2005;25(1–2):231–61.
- [30] Gallouët T, Hérard JM, Seguin N. Some approximate Godunov schemes to compute shallow water equations with topography. *Comput Fluids* 2003;32(4):479–513.
- [31] Halpern L, Rauch J. Absorbing boundary conditions for diffusion equations. *Numer Math* 1995;71(2):185–224.
- [32] Huang A, Temam R. The linearized 2d inviscid shallow water equations in a rectangle: boundary conditions and well-posedness. submitted for publication. arXiv:1209.3194.
- [33] Huang A, Temam R. The nonlinear 2d subcritical inviscid shallow water equations with periodicity in one direction; in preparation (under completion).
- [34] Huang A, Petcu M, Temam R. The nonlinear 2D supercritical inviscid shallow water equations in a rectangle; submitted for publications.
- [35] Kurganov A, Tadmor E. New high-resolution central schemes for nonlinear conservation laws and convection–diffusion equations. *J Comput Phys* 2000;160(2):720–42.
- [36] Kurganov A, Petrova G. A third-order semi-discrete genuinely multidimensional central scheme for hyperbolic conservation laws and related problems. *Numer Math* 2001;88:683–729.
- [37] Kurganov A, Noelle S, Petrova G. Semidiscrete central upwind schemes for hyperbolic conservation laws and Hamilton–Jacobi equations. *SIAM J Sci Comput* 2001;23(3):707–40.
- [38] Kurganov A, Levy D. Central-upwind schemes for the Saint-Venant system. *M2AN* 2002;36(3):397–425.
- [39] Ra J. LeVeque finite volume methods for hyperbolic problem. V. 31, Cambridge Texts in Applied Mathematics; 2002.
- [40] McDonald A. Transparent boundary conditions for the shallow water equations: testing in a nested environment. *Mon Weather Rev* 2003;131:698–705.
- [41] Marion M, Temam R. Nonlinear Galerkin methods. *SIAM J Numer Anal* 1989;26:1139–57.
- [42] Marion M, Temam R. Navier–Stokes equations. Theory and approximation. In: Ciarlet PG, Lions JL, editors. Handbook of numerical analysis, vol. VI. Amsterdam: North-Holland; 1998. p. 503–689.
- [43] Nycander J, Hogg A McC, Frankcombe LM. Open boundary conditions for nonlinear channel flow. *Ocean Modell* 2008;24:108–21.
- [44] Navon IM, Neta B, Hussaini MY. A perfectly matched layer approach to the linearized shallow water equations models. *Mon Weather Rev* 2004;132:1369–78.
- [45] Palma E, Matano R. On the implementation of passive open boundary conditions for a general circulation model: the barotropic mode. *J Geophys Res* 1998;103:1319–41.
- [46] Petcu M, Temam R. The shallow water equations with Dirichlet boundary conditions. *Discrete Contin Dyn Syst* 2011;4(1).
- [47] Petcu M, Temam R. The one-dimensional shallow water equations with transparent boundary conditions. *Math Methods Appl Sci (MMAS)*; 2011. doi:10.1002/mma1482.
- [48] Petcu M, Temam R. An interface problem: the two-layer shallow water equations. *DCDS-A* 2013;6(2):401–22. <http://dx.doi.org/10.394/dcds2013.6.401>.
- [49] Strikwerda JC. Finite difference schemes and partial differential equations. 2nd ed. SIAM; 2007.
- [50] Shiue M-C, Laminie J, Temam R, Tribbia J. Boundary value problems for the shallow water equations with topography. *J Geophys Res* 2011;116:C02015.
- [51] Svard M, Gong J, Nordstrom J. Stable artificial dissipation operators for finite volume schemes on unstructured grids. NIA; 2005.
- [52] Temam R. Inertial manifolds and multigrid methods. *SIAM J Math Anal* 1990;21:154–78.
- [53] Temam R. Multilevel methods for the simulation of turbulence. A simple model. *J Comput Phys* 1996;127(2):309–15.
- [54] Temam R, Tribbia J. Open boundary conditions for the primitive and Boussinesq equations. *J Atmos Sci* 2003;60:2647–60.
- [55] Treguier AM, Barnier B, de Miranda AP, Molines JM, Grima N, Imbard M, et al. An eddy-permitting model of the Atlantic circulation: evaluating open boundary conditions. *J Geophys Res* 2001;106:22115–29.
- [56] Wesseling P. Principles of computational fluid dynamics, vol. 29. Springer; 2009.
- [57] Whitham B. Linear and nonlinear waves. Pure and applied mathematics (New York). New York: A Wiley-Interscience Publication. John Wiley & Sons, Inc.; 1999.
- [58] Warner P, Peterson R, Treadon R. A tutorial on lateral boundary conditions as a basic and potentially serious limitation to regional numerical weather prediction. *Bull Am Meteor Soc* 1997;78:2599–617.